JGR Oceans

RESEARCH ARTICLE
10.1029/2021JC017315

Modeling the Impact of Macrozooplankton on Carbon Export Production in the Southern Ocean

Onur Karakuş[1], Christoph Völker[1], Morten Iversen[1], Wilhelm Hagen[2,3], Dieter Wolf-Gladrow[1], Bettina Fach[4], and Judith Hauck[1]

[1]Alfred-Wegener-Institut, Helmholtz-Zentrum für Polar- und Meeresforschung, Bremerhaven, Germany, [2]University of Bremen, BreMarE, Marine Zoology, Bremen, Germany, [3]University of Bremen, MARUM Center of Environmental Sciences, Bremen, Germany, [4]Middle East Technical University, Institute of Marine Sciences, Erdemli-Mersin, Turkey

Abstract Macrozooplankton and its grazing pressure shape ecosystem structures and carbon pathways in the Southern Ocean. Here, we present the implementation of "polar macrozooplankton" as a plankton functional type and a related fast-sinking detritus class (fecal pellets) into the biogeochemical model REcoM-2. We use the model to assess major carbon pathways and ecosystem structure in the Southern Ocean south of 50°S. The model represents zooplankton biomass and its spatial distribution in the Southern Ocean reasonably well in comparison to available biomass data. A distinct difference of our model from previous versions is the seasonal pattern of particle formation processes and ecosystem structures in the Southern Ocean. REcoM-2 now captures high zooplankton biomass and a typical shift from a dominance of phytodetrital aggregates in spring to zooplankton fecal pellets later in the year. At sites with high biomass of macrozooplankton, the transfer efficiency of particulate organic carbon can be as high as 50%, and the carbon content of the exported material increases. In our simulations, macrozooplankton is an important component of the Southern Ocean plankton community, contributing up to 0.12 Pg C per year (14%) to total modeled carbon export across 100 m depth. Macrozooplankton changes the phytoplankton composition and supports the recycling of macronutrients. These results support the important role of macrozooplankton such as krill in the Southern Ocean and have implications for the representation of Southern Ocean biogeochemical cycles in models.

Plain Language Summary Large zooplankton such as krill is an important component of marine ecosystems, but it is rarely represented in ocean ecosystem models. Large zooplankton grazes on phytoplankton, smaller zooplankton, and sinking particles in the ocean. To understand the role of large zooplankton for carbon cycling in the Southern Ocean, we have implemented this group into our ecosystem model and describe macrozooplankton feeding and particle formation based on observations. We find that large zooplankton supports a stable or even increased growth of phytoplankton, in spite of its grazing. This is because it also returns nutrients to phytoplankton via excretion. Besides, large zooplankton increases the transfer of carbon to the deep ocean.

Key Points:

- A new macrozooplankton parametrization is implemented into the biogeochemical model REcoM-2
- Transfer efficiency reaches up to 50% due to the high carbon content and fast sinking of macrozooplankton fecal pellets
- Macrozooplankton contributes up to 14% (0.12 Pg C yr^{-1}) to modeled carbon export at 100 m depth in the Southern Ocean south of 50°S

Supporting Information:

Supporting Information may be found in the online version of this article.

Correspondence to:

O. Karakuş,
onur.karakus@awi.de

Citation:

Karakuş, O., Völker, C., Iversen, M., Hagen, W., Wolf-Gladrow, D., Fach, B., & Hauck, J. (2021). Modeling the impact of macrozooplankton on carbon export production in the Southern Ocean. *Journal of Geophysical Research: Oceans*, *126*, e2021JC017315. https://doi.org/10.1029/2021JC017315

Received 26 FEB 2021
Accepted 1 NOV 2021

1. Introduction

The biological carbon pump plays an essential role in the cycling of carbon in the oceans (Honjo, 2004; Volk & Hoffert, 1985). It is driven by a large variety of organisms that are part of a complex ecosystem. The export of organic carbon from the surface to deeper layers proceeds via several pathways including the formation of aggregates and fecal pellets that sink gravitationally, and the downwelling of dissolved compounds (Boyd et al., 2019; Steinberg & Landry, 2017). Marine carbon cycle models are used to assess carbon fluxes in the ocean ecosystems to gain a deeper understanding of the carbon cycle. However, the complexity of marine ecosystems and the processes relevant for carbon export cannot be fully reflected in these models (Laufkötter et al., 2016). For example, zooplankton is still represented by a single variable in many global ocean biogeochemical models (Séférian et al., 2020), despite the large diversity and traits of zooplankton. A handful of models represent three plankton functional types (PFTs) of zooplankton (Le Quéré et al., 2016; Stock et al., 2020).

One of the zooplankton PFTs is macrozooplankton, defined as the size class of 2–20 cm, which reaches high biomass and shows a patchy distribution (Moriarty et al., 2013). Groups being classified as macrozooplankton

are, for example, euphausiids, but also pelagic members of, for example, cnidarians, amphipods, and decapods. They consume a large spectrum of prey sizes with different feeding strategies and carbon assimilated by this group is transferred to higher trophic levels, transforming and transferring particulate organic carbon (Steinberg & Landry, 2017). They produce large fecal pellets with a high sinking rate, which reduces microbial degradation in the euphotic zone and leads to direct sinking to the meso- and bathypelagic (Turner, 2002). The relative contribution of zooplankton fecal pellets to the particulate organic carbon (POC) flux can comprise up to 100% in different sites of the ocean, illustrating the important role of zooplankton in the biological carbon pump (Turner, 2015).

The Southern Ocean is one of the regions, which plays a significant role in the export of particulate organic carbon (Arteaga et al., 2018; Schlitzer, 2002). Export production (EP), an important component of the biological carbon pump, transfers 15%–25% of the carbon fixed by primary production to deeper waters in the Southern Ocean (Henson et al., 2012). The estimation of export production over the 100 m depth horizon varies between 10 to 600 mg C m^{-2} d^{-1} with an average of around 150 mg C m^{-2} d^{-1} (Maiti et al., 2013). The biogenic carbon flux is dominated by the gravitational sinking of phytodetrital aggregates and zooplankton fecal pellets, although other processes such as the sinking of zooplankton carcasses, molts, and zooplankton migration also contribute (Boyd et al., 2019; Halfter et al., 2020). The relative contributions of phytodetrital aggregates and zooplankton fecal pellets to carbon export show seasonal and spatial patterns (Dagg et al., 2003; Ebersbach & Trull, 2008; Halfter et al., 2020; Iversen et al., 2017; Laurenceau-Cornec et al., 2015; Turner, 2015). For example, phytodetrital aggregates are reported to contribute 24%–74% to the export production in the Kerguelen Plateau (Ebersbach & Trull, 2008) and the relative contribution of zooplankton fecal pellets can vary from 22%–63% in spring to 2%–7% in summer in the Pacific Antarctic Polar Front region (Dagg et al., 2003). Generally, a high contribution of aggregates is related to phytoplankton blooms in the surface waters (Turner, 2015), although phytodetrital aggregates can also dominate the export flux in the Southern Ocean high-nutrient low-chlorophyll (HNLC) waters where grazing pressure is relatively low (Halfter et al., 2020). At the naturally iron-fertilized Kerguelen Plateau, a shift occurred from dominance of phytodetrital aggregates in spring to zooplankton fecal pellets later in the year (Ebersbach & Trull, 2008; Laurenceau-Cornec et al., 2015; Rembauville et al., 2015).

The Southern Ocean also hosts a high density of macrozooplankton, including the efficient grazer Antarctic krill (*Euphausia superba*) with biomass estimates ranging between 60 to 420 million tons based on acoustic and in situ (net haul density and length frequency) data (Atkinson et al., 2009; Nicol et al., 2000; Siegel et al., 2004). Krill shape the ecosystem, for example, through stimulating primary productivity with the release of iron and ammonium and affect the carbon export (Cavan et al., 2019). Furthermore, krill impact the accumulation of diatoms due to grazing, which consequently plays a decisive role in biogeochemical cycles (Smetacek et al., 2004). Krill enable short pathways between lowest (phytoplankton) and higher trophic levels (marine mammals) and contribute to an efficient carbon transfer to the deeper layers via fecal pellet production (Meyer, 2012). While the contribution of krill to particulate organic carbon production may vary between 7 and 1,300 mg C m^{-2} d^{-1} in the Southern Ocean (Belcher et al., 2019; Clarke et al., 1988), krill fecal pellets contribute on average 0.04 Pg C per yr^{-1} which equals 35% of the total export flux in the marginal ice zone (Belcher et al., 2019).

Large-scale ocean biogeochemical models differ from each other in terms of complexity, such as the number of functional types of phyto- and zooplankton and represented processes (Laufkötter et al., 2016; Le Quéré et al., 2016; Séférian et al., 2020). Due to a lack of mechanistic understanding, projections of the future biological carbon pump are associated with much larger uncertainties compared to physical and chemical variables, such as temperature, oxygen, or pH (Frölicher et al., 2016). Zooplankton groups and their parameterizations play a critical role in the performance of ecosystem models with respect to primary production (Le Quéré et al., 2016), secondary production (Anderson et al., 2013), and particulate organic carbon production and export (Laufkötter et al., 2016). Growth, transport, and impact of macrozooplankton, especially krill, have been simulated in various regional models (Arrigo et al., 2003; Fach et al., 2002; Hense et al., 2003; Hofmann & Lascara, 2000; Lancelot et al., 2000), but only a few global biogeochemical models possess representations of macrozooplankton (Le Quéré et al., 2016; Stock et al., 2014).

Here, we present a new version of the global ocean ecosystem and biogeochemistry model REcoM-2 with the implementation of a macrozooplankton group. Up to now, REcoM-2 included a single type of zooplankton

which, based on the chosen parameterization, represented small and fast-growing zooplankton. The goal of the current paper is to analyze the effect of an additional macrozooplankton group that can create large biomass accumulations in certain regions and thereby impact the structure and functioning of ecosystems. The parameterization for this second zooplankton group is based on the temperature tolerance of Antarctic krill, hence, this group cannot represent macrozooplankton in warmer waters. The aim is therefore mainly to obtain a more realistic representation of the Southern Ocean biological carbon pump in the model. We implemented this new group and parameterized it as a macrozooplankton group resembling Antarctic krill for the following reasons: (a) the occurrence of high biomass of macrozooplankton (Antarctic krill) in the Southern Ocean (Atkinson et al., 2004) and its specific role in biogeochemical cycling as characterized by (b) the slow growth rates of this group (Le Quéré et al., 2016), (c) the efficient filter-feeding of krill (Meyer, 2012), and (d) a fecal pellet production with strong transfer efficiency to the deep ocean (Belcher et al., 2017). In this study, we analyze carbon export pathways and the role of macrozooplankton in the Antarctic ecosystem with and without this group.

2. Methods

2.1. FESOM-REcoM With Macrozooplankton and Two Sinking Particle Classes

We used the Finite Element Sea Ice Ocean Model FESOM-1.4 (Wang et al., 2014) as the physical component of the coupled ocean-ecosystem model. FESOM-1.4 uses the finite element method for solving the primitive equations on an unstructured mesh which allows calculations with higher resolutions in more dynamical areas and coarser resolution in less dynamic, for example, subtropical areas. In this study, we used the CORE-II mesh set-up which has a resolution of 20 km along the Antarctic coast and around 70 km at 60°S (Sidorenko et al., 2011). The model set-up and its performance is described by Sidorenko et al. (2011), and evaluated as part of the coordinated ocean-ice reference experiments phase II (CORE-II) globally (e.g., Griffies et al., 2014) and regionally (see Downes et al., 2015, 2018; Farneti et al. (2015) for Southern Ocean specific analyses). A multi model comparison of sea-ice extent and concentration, including FESOM-1.4, was discussed in Downes et al. (2015). As reported there, FESOM simulates a reasonable seasonal cycle of sea-ice extent, with a realistic representation of the maximum extent. A notable caveat is a low extent in March, which is shared with all other models in their study. FESOM was reported to have the smallest sea-ice concentration bias of all models in March. Downes et al. (2015) do not compare sea-ice thickness as thickness and concentration correlate positively. Exemplarily, we show sea-ice extent and thickness in Figure S5 in Supporting Information S1. Sea ice extent reaches its maximum in September and its minimum in March, in agreement with remote sensing studies (Comiso & Nishio, 2008). The mean sea ice thickness varies between a minimum of 0.75 m in April and a maximum of 1.06 m in November in the model. The thickest sea ice (>2 m) is in the Weddell Sea, the Bellingshausen and Amundsen Seas, the western Ross Sea, and along the Antarctic coastline. The thinnest ice occurs in the eastern Weddell Sea, and in the Indian and Pacific sectors (Figure S5 in Supporting Information S1), in reasonable agreement with Kurtz and Markus (2012).

The Regulated Ocean Ecosystem Model (Hauck et al., 2013; Schourup-Kristensen et al., 2014; REcoM-2) is the biogeochemical component of the coupled system. It represents the carbonate system, two phytoplankton classes (nanophytoplankton and diatoms), and one zooplankton group representing a fast-growing small zooplankton group (Figure 1a). It resolves the cycling of the nutrients nitrate (DIN), silicic acid (DSi), and iron (DFe). Phytoplankton stoichiometry is allowed to vary with environmental conditions (variable N:C:Chl:Si for diatoms and N:C:Chl for nanophytoplankton). Sinking particles have three sources in the original set-up: aggregation of primary producers, sloppy feeding (which implicitly also includes defecation), and mortality of the zooplankton group. A skill assessment of the biogeochemical model's original version is presented by Schourup-Kristensen et al. (2014). The model version used in this study resembles the version assessed in Schourup-Kristensen et al. (2014) with minor changes as described in the following. Total global net primary production (NPP) is 30.1 Pg C yr^{-1} and EP at 100 m is 5.1 Pg C yr^{-1} (31.6 and 6.1 Pg C yr^{-1}, respectively, in Schourup-Kristensen et al., 2014). The photodamage parameterization by Álvarez et al. (2018) is used and leads to a larger share of diatoms (Figure S6 in Supporting Information S1) in the Southern Ocean compared to Schourup-Kristensen et al. (2014). As a result, the Southern Ocean DIN bias is reduced compared to Schourup-Kristensen et al. (2014) and the silicic acid bias is negative, highlighting the sensitivity of the model to chlorophyll loss process parameterization and parameters. In this study, we

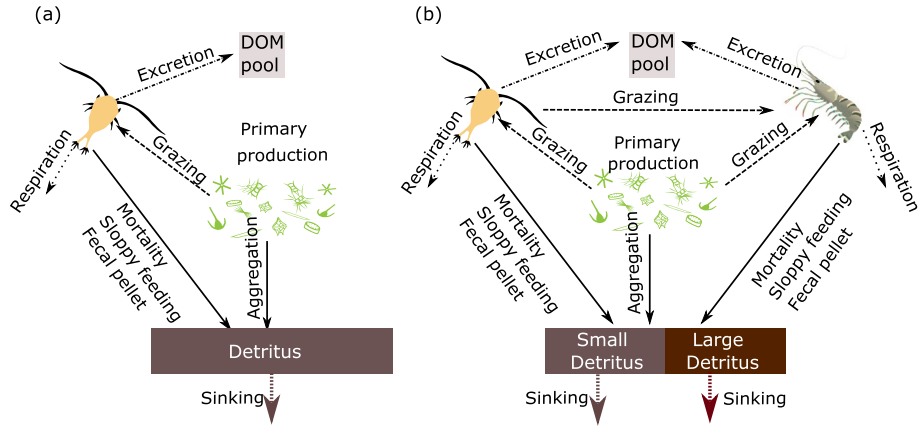

Figure 1. Processes in biogeochemistry model (a) REcoM-2, (b) REcoM-2-M with two zooplankton groups and a second, large detritus class. Both model versions represent primary production by two phytoplankton classes (nanophytoplankton and diatoms) and a small and fast-growing zooplankton group. In both versions, sinking detritus is produced via phytoplankton aggregation and through small zooplankton mortality, and a loss term accounting for sloppy feeding and fecal pellet production. Other loss processes for zooplankton biomass are respiration and excretion of dissolved organic matter. In addition, REcoM-2-M explicitly represents macrozooplankton with losses of sinking particulate organic matter being routed to a large detritus class with a higher sinking speed. The loss through fecal pellets is represented explicitly and macrozooplankton respiration varies in response to the seasonal cycle.

implemented an additional macrozooplankton group and a new detritus group representing large particles (Figure 1b). Also, fecal pellet production was added as an explicit loss term for the new macrozooplankton group (Figure 1b). The set-up of REcoM-2 further differs from previous model descriptions (Hauck et al., 2013; Schourup-Kristensen et al., 2014) by using a temperature-dependent respiration rate with a rate constant of 1% of biomass per day (Le Quéré et al., 2016) for the small zooplankton group, and by considering the effect of diatom nutrient limitation on stickiness and consequently on the aggregation rate (Aumont et al., 2015; Waite et al., 1992, Equation 7).

2.2. Macrozooplankton in FESOM-REcoM

The new macrozooplankton group was parameterized based on the characteristics of Antarctic krill. Nevertheless, we refer to this group as macrozooplankton since it will also cover other niches in the model, as long as these other types (e.g., salps) are not modeled explicitly. Furthermore, not all details of krill are covered here (e.g., life cycle, vertical migration). Macrozooplankton is described by the two-state variables nitrogen (N_{macro}) and carbon (C_{macro}) as shown in differential Equations 1 and 2. Grazing is the single source for macrozooplankton biomass and mortality, excretion, respiration, and fecal pellet production are the loss terms.

$$\underbrace{\frac{dN_{macro}}{dt}}_{\text{nitrogen pool}} = \underbrace{G \cdot \gamma}_{\text{grazing}} - \underbrace{m \cdot N_{macro}^2}_{\text{mortality}} - \underbrace{\epsilon_N \cdot N_{macro}}_{\text{excretion}} - \underbrace{f_N \cdot G}_{\text{fecal pellet}} \tag{1}$$

$$\underbrace{\frac{dC_{macro}}{dt}}_{\text{carbon pool}} = \underbrace{(\sum_i \frac{1}{q_i} \cdot G_i) \cdot \gamma}_{\text{grazing}} - \underbrace{\frac{1}{q} \cdot m \cdot N_{macro}^2}_{\text{mortality}} - \underbrace{\epsilon_C \cdot C_{macro}}_{\text{excretion}} - \underbrace{r \cdot C_{macro}}_{\text{respiration}} - \underbrace{f_C \cdot G_C}_{\text{fecal pellet}} \tag{2}$$

In Equation 1, grazing efficiency (assimilation efficiency) γ determines the fraction of total grazing (G) by macrozooplankton that is converted into macrozooplankton biomass (Equation 3). To mimic predation by higher trophic levels and natural mortality of the macrozooplankton, mortality of the macrozooplankton is described by a quadratic term of the concentration N_{macro} where m is the mortality rate constant ($m \cdot N_{macro}^2$). Nitrogen excretion is determined by the excretion rate constant ϵ_N and is proportional to the N_{macro} biomass. The fecal pellet production rate is described as a function of the total grazing G and the fecal pellet production rate constant (f_N) that determines how much of the grazing fraction is transferred into the larger detritus class nitrogen pool. Equation 2 shows the state variable carbon of the macrozooplankton group. The grazing flux in nitrogen units (G) is converted into

Table 1
Chosen Parameter Values for the Representation of Macrozooplankton in REcoM-2-M

Parameter	Symbol	Value (unit)	Reference
Maximum grazing rate	ε	0.1 (d^{-1})	Hofmann and Lascara (2000)
Grazing efficiency	γ	0.8 (dimensionless)	Fach et al. (2002)
Respiration rate constant	r	0.01 (d^{-1})	Hofmann and Lascara (2000)
Mortality rate constant	m	0.003 (d^{-1})	Fach et al. (2002)
N excretion rate constant	ϵ_N	0.02 (d^{-1})	Atkinson et al. (2002)
C excretion rate constant	ϵ_C	0.02 (d^{-1})	Atkinson et al. (2002)
Half saturation constant	σ	0.01 ((mmol N m^{-3})^2)	Meyer et al. (2009)
Initial grazing preference for diatoms	p'_{dia}	1 (dimensionless)	see Section 2.2
Initial grazing preference for nanophy.	p'_{nano}	0.5 (dimensionless)	see Section 2.2
Initial grazing preference for heterotrophs	p'_{zoo}	0.8 (dimensionless)	see Section 2.2
Initial grazing preference for detritus groups	p'_{det}	0.5 (dimensionless)	see Section 2.2
N fecal pellet production rate constant	f_N	0.13 (d^{-1})	see Section 2.2
C fecal pellet production rate constant	f_C	0.295 (d^{-1})	see Section 2.2

carbon units using the respective intracellular N:C ratios (q_i) of each food source (i = diatom, nanophytoplankton, small zooplankton group, detritus classes). The quadratic mortality is converted to carbon using the intracellular macrozooplankton N:C ratio (q). The excretion rate constant (ϵ_C) determines the loss of carbon to the dissolved organic carbon pool and the respiration rate ($r \cdot C_{macro}$) describes the loss of carbon to the dissolved inorganic carbon pool. The fecal pellet production rate constant (f_C) and the grazing rate G together determine the fraction of carbon being lost to the large detritus carbon pool via fecal pellets.

$$G = \varepsilon \cdot \frac{\left(\sum_i p_i \cdot N_i\right)^2}{\sigma + \left(\sum_i p_i \cdot N_i\right)^2} \cdot f_T \cdot N_{macro} \tag{3}$$

$$p_i = \frac{p'_i \cdot N_i}{\sum_i p'_i \cdot N_i} \tag{4}$$

Grazing of the macrozooplankton group is described by the Holling type III ingestion function (Equation 3) on small zooplankton (i = 1), diatoms (i = 2), nanophytoplankton (i = 3), and both detritus classes (i = 4, 5) using the relative grazing preferences (p_i) by Fasham et al. (1990) (Equation 4). Since overwintering krill can switch to different food sources and graze on phytodetritus (Meyer, 2012), we implemented grazing on detritus groups by macrozooplankton. The maximum grazing rate (ε) is set to 0.1 d^{-1} (Hofmann & Lascara, 2000) and the half saturation constant (σ) is 0.01 (mmol N m^{-3})^2, based on Meyer et al. (2009). It is generally accepted that diatoms are the main food source for krill, but they also feed on copepods (Schmidt et al., 2014). In this study, the initial grazing preferences (p'_i) are taken as 1, 0.5, 0.8, and 0.5 for diatoms, nanophytoplankton, small zooplankton group and detritus groups respectively. Relative grazing preferences (p_i, i = each food source) are calculated as division of each food source ($p'_i \cdot N_i$) by the total food ($\sum_i p'_i \cdot N_i$). All parameter values for macrozooplankton are summarized in Table 1.

Macrozooplankton grazing varies with temperature. The following parameterization is applied (Butzin & Pörtner, 2016, Equation 5, Figure 2),

$$f_T = \frac{\exp\left(\frac{Q_a}{T_r} - \frac{Q_a}{T}\right)}{1 + \exp\left(\frac{Q_h}{T_h} - \frac{Q_h}{T}\right)} \tag{5}$$

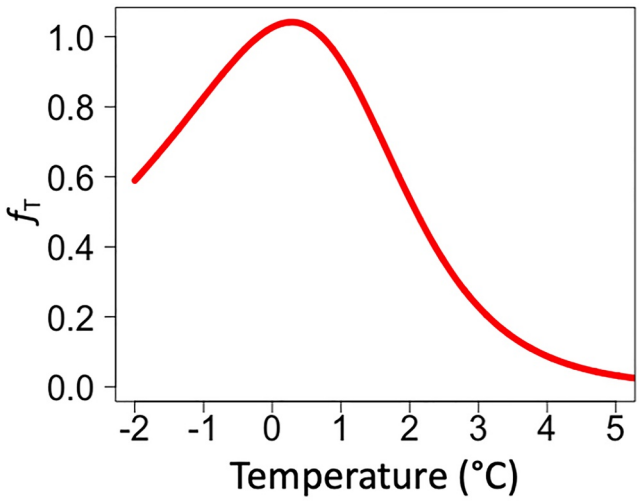

Figure 2. Exponential temperature function (dimensionless) adapted from Butzin and Pörtner (2016) for macrozooplankton grazing (see Equation 5) with an optimum temperature for macrozooplankton growth at 0.5°C (Atkinson et al., 2006).

where T (K) is absolute temperature, T_r and T_h represent the intrinsic optimum temperature for development. Inhibitive processes dominate outside this temperature window. Q_a and Q_h are the temperatures for the uninhibited and inhibited reaction kinetics, respectively (Butzin & Pörtner, 2016). The parameter values were chosen as $T_r = 272.5$ K, $T_h = 274.5$ K, $Q_a = 28{,}145$ K, and $Q_h = 105{,}234$ K to represent the temperature sensitivity of daily growth rates with the maximum growth of krill occurring at 0.5°C as described in Atkinson et al. (2006).

Mortality, sloppy feeding, and fecal pellet production are the processes through which macrozooplankton forms detrital particles. The mortality rate constant m is set to 0.3% per day (Fach et al., 2002) in a quadratic formulation (Equation 1) and $1 - \gamma = 20\%$ of the grazed material is transferred to the detritus pool through sloppy feeding (Fach et al., 2002). Fecal pellet production was set to 29% of grazing flux in carbon units and 13% of grazing flux in nitrogen units to be consistent with the observed high C:N ratio of around 13 in krill fecal pellets (Atkinson et al., 2012). The excretion rate constant of dissolved organic carbon and nitrogen is taken as 2% per day from Atkinson et al. (2002).

The daily respiration rate constant (r) of macrozooplankton in the model depends on the season and grazing activity and a standard respiration rate (R_s, Equation 6, Hofmann & Lascara, 2000).

$$r = R_s \cdot (1 + R_f + R_a) \tag{6}$$

The term respiration activity factor (R_a) accounts for reduced krill respiration rates in winter. R_a is set to −0.5 from Julian day 150 through 250 (southern hemisphere winter) which represents a 50% metabolic reduction. We chose to make respiration rates dependent on Julian day because the metabolic activity of krill is affected by the Antarctic light regime (Meyer, 2012; Teschke et al., 2007), which in the model is tied to Julian Day. The feeding activity factor (R_f) represents the metabolic cost of feeding activity and depends on the daily ratio of grazing flux to carbon biomass of macrozooplankton. It increases linearly from 0 to 1 for daily grazing to biomass ratio between 0% and 10% and remains constant at 1 for ratios above 10%. The standard respiration rate (R_s) is set to 1% per day (Hofmann & Lascara, 2000).

2.3. Two Sinking Particle Classes and Particulate Organic Carbon Production in FESOM-REcoM

To better represent macrozooplankton-related export processes, we implemented a second detritus class which represents large, fast-sinking particles. Mortality, sloppy feeding, and fecal pellet production by the macrozooplankton group are the only sources for the large detritus class in REcoM-2-M (Figure 1b). In the Scotia Sea, sinking rates of krill fecal pellets ranged between 27 and 1,218 m d^{-1} with a median value of 304 m d^{-1} (Atkinson et al., 2012). In REcoM-2-M, a constant sinking rate of 200 m d^{-1} was set for the large detritus. In the control simulation, there is only one detritus class (Figure 1a) with an initial sinking speed of 20 m d^{-1} at the surface which increases linearly with depth until reaching a maximum sinking rate of 170 m d^{-1} at the depth of 5,300 m depth. This detritus class represents smaller particles formed by aggregation of phytoplankton and processes related to the small zooplankton group (mortality and sloppy feeding) in the simulations with two detritus classes.

In this study, we refer to sinking particulate organic carbon (sPOC) as dead material which is transferred into the detritus pool. Processes that lead to sPOC production are an aggregation of phytoplankton, sloppy feeding, mortality of zooplankton, and the fecal pellet production by macrozooplankton in our modeling experiments. Aggregation of phytoplankton is calculated in two steps. First, the aggregation rate constant (a, unit: d^{-1}, Equation 7) is calculated from the specific aggregation rate constants for phytoplankton (a_{pp}) and detritus (a_{pd}). The effect of increased stickiness of diatoms under nutrient limitation (Aumont et al., 2015; Waite et al., 1992) is taken into account by multiplication with (1 - L^D_{lim}) where L^D_{lim} is the nutrient limitation factor which ranges between 0 under

Table 2
Processes Included (X) in Model Experiments With Increasing Complexity of Macrozooplankton Representation

Simulation	Macrozooplankton	Large detritus	Detritus grazing	Fecal pellet production
CTRL	–	–	–	–
MACROZOO	X	–	–	–
MACROZOO_2DET	X	X	–	–
MACROZOO_DETGRAZ	X	X	X	–
MACROZOO_ALL	X	X	X	X

strong nutrient limitation, and 1 when nutrients are replete. Second, total aggregation ($sPOC_{phy}^{prod}$) is calculated from the phytoplankton biomass (*PhyC, DiaC*) and the aggregation rate constant (Equation 8).

$$a = a_{pd} \cdot DetN + a_{pp} \cdot PhyN + a_{pp}(1 - L_{\text{lim}}^{D}) \cdot DiaN \tag{7}$$

$$sPOC_{phy}^{prod} = a \cdot PhyC + a \cdot DiaC \tag{8}$$

Another important source for sPOC comes through both zooplankton groups in REcoM-2-M. The sPOC production from sloppy feeding, mortality and fecal pellet production (Equation 9) are described for macrozooplankton in Section 2.2, equations (Equations 1 and 2). Fecal pellet production is only represented explicitly for the macrozooplankton group. The sPOC production from sloppy feeding is calculated by multiplication of the grazing fluxes in carbon units ($\sum_i \frac{1}{q_i} \cdot G_i$) with the one minus grazing efficiency term (γ) for macrozooplankton. The small zooplankton group contributes to sPOC formation by mortality and sloppy feeding, which implicitly includes fecal pellets (Equation 10).

$$sPOC_{zoo}^{prod} = sPOC_{zoo}^{mortality} + sPOC_{zoo}^{sloppyfeeding} + sPOC_{macrozoo}^{fecalpellet} \tag{9}$$

$$sPOC_{zoo}^{sloppyfeeding} = \underbrace{\left(\sum_i \frac{1}{q_i} \cdot G_i\right) \cdot (1 - \gamma)}_{\text{Macrozoo.}} + \underbrace{\left(\sum_i \frac{1}{q_i} \cdot G_{i,\,\text{zoo1}}\right) \cdot (1 - \gamma_{\text{zoo1}})}_{\text{Small zoo.}} \tag{10}$$

2.4. Model Setup and Simulations

The global model was forced with the JRA-55-do atmospheric forcing data set version 1.3.1 (Kobayashi et al., 2015) in a 60 years long simulation. Repeated year forcing fields from the year 1961 of surface downwelling short and long-wave radiation, surface rainfall, and snowfall fluxes as well as near-surface (2 m) air temperature, specific humidity, eastward and northward wind components, and sea level pressure were used. Freshwater runoff and the surface salinity field for a weak surface salinity restoration (Sidorenko et al., 2011) are taken from the CORE-II climatology (Griffies et al., 2009). The nutrients dissolved inorganic nitrogen and dissolved silicic acid were initialized with World Ocean Atlas 2013 products (Garcia et al., 2013), and dissolved inorganic carbon (DIC) and alkalinity from GLODAPv2 (Lauvset et al., 2016). We performed global model simulations, but only analyzed the Southern Ocean. The last 5 years of the model simulation were analyzed with respect to nutrient concentrations, net primary production, export production at 100 m, particulate organic carbon production, and ecosystem structure south of 50°S. Export production was calculated by multiplying detritus concentration at 100 m with the sinking speed at 100 m.

We conducted five simulations to analyze the effects of different processes within the newly implemented macrozooplankton group (Table 2). First, the control simulation (CTRL) was conducted with the original setup with only one zooplankton group of REcoM-2. Further, we executed four simulations with the increasing complexity of macrozooplankton representation. These simulations include (a) only the new macrozooplankton group (MACROZOO), (b) a simulation with macrozooplankton and a second detritus pool (MACROZOO_2DET), (c) another including in addition detritus grazing (MACROZOO_DETGRAZ), and (d) a final one including

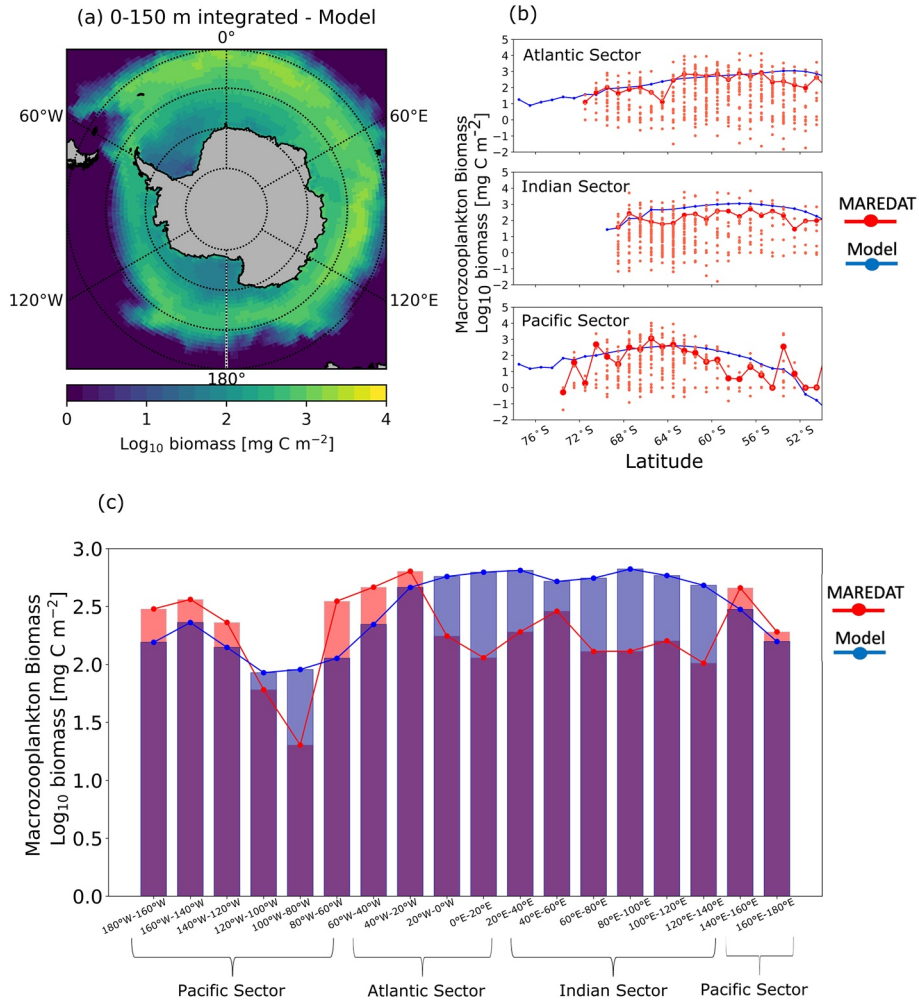

Figure 3. Modeled macrozooplankton biomass, presented as vertically-integrated (0–150 m), and annually averaged log10 biomass [mg C m^{-2}] in the Southern Ocean (a) spatial distribution, (b) Zonal mean of biomass in Atlantic, Indian and Pacific sectors for model (dots with blue line) and MAREDAT (dots with red line, small dots indicate individual data points, and larger dots the mean), (c) Spatial mean of the region within each 20° longitude bin in the Southern Ocean for model and MAREDAT data. The light red areas and light blue areas in the bars show underestimation and overestimation of the model compared to data, respectively.

also fecal pellet production (MACROZOO_ALL). In the results Section 3.1 we focus only on the evaluation of the MACROZOO_ALL simulation, and in Section 3.2 and 3.3, we focus on the comparison of the CTRL and MACROZOO_ALL simulations. In Section 3.4, we analyze the effect of the different processes on NPP, EP, and sPOC production using all simulations.

2.5. Evaluation of Modeled Macrozooplankton Biomass

To evaluate the macrozooplankton biomass results, we used the MAREDAT global macrozooplankton dataset, covering the period from 1926 to 2010 (Moriarty et al., 2013). Since there is no data in the MAREDAT data set for the austral winter months July to September, these months were also excluded for the biomass comparison from the model output. The modeled annual mean (October–June) macrozooplankton biomass from the last five model years 2013–2017 was interpolated to the MAREDAT data grid (1° × 1°). We restricted the comparison to the Southern Ocean south of 50°S. Here, the comparison focuses on two aspects: (a) the spatial mean of macrozooplankton biomass for the model and MAREDAT and (b) the depth-integrated macrozooplankton distribution integrated over the upper 150 m for model and data (Figure 3). Furthermore,

the statistical distribution of macrozooplankton biomass where we subsampled the model for MAREDAT data points considering different depth ranges is summarized in Table S1 in Supporting Information S1.

3. Results

3.1. Macrozooplankton Biomass in the Southern Ocean

The order of magnitude of the mean biomass is captured well, although the model mean (2.55 mg C m^{-3}) is lower than the MAREDAT (Moriarty et al., 2013) mean (5.25 mg C m^{-3}, Table S1 in Supporting Information S1). This is caused by some very high biomass numbers in MAREDAT, being reflected in a maximum annual mean of 582.3 mg C m^{-3} which are not captured by the model with a maximum annual mean of 23.5 mg C m^{-3} derived from the subsampled model. This might to some extent reflect a sampling and reporting bias with more observations at locations with high biomass. The integrated modeled macrozooplankton biomass is 2.81 Tg C which is closer to 3.07 Tg C in observations (Table S1 in Supporting Information S1).

When integrating over the whole Southern Ocean, the mean biomass of the modeled macrozooplankton over the upper 150 m is 367.2 mg C m^{-2}. While this would suggest an underestimation of the modeled macrozooplankton biomass as compared to the MAREDAT mean biomass of 495.9 mg C m^{-2}, the sampling bias needs to be taken into account. When subsampling the model according to the data points in MAREDAT including their same depth range, the mean biomass equals 517.5 mg C m^{-2}, which is reasonably close to the MAREDAT numbers. The modeled macrozooplankton biomass decreases with depth. While 98.4% of the modeled biomass is within the upper 150 m, 74.3% is between 0 and 50 m. While there is some available data below 150 m in MAREDAT (max. 120.4 mg C m^{-3}), the model does not reproduce biomass below 150 m. This is expected since the vertical migration of macrozooplankton is not represented.

We further investigate the spatial distribution of macrozooplankton biomass. In MAREDAT, the observations are denser around the Antarctic Peninsula than at other sites in the Southern Ocean. In the upper 150 m, 39% of all observations were obtained between 0°W and 80°W, and 39% of them between 0°W and 120°E, making the Pacific sector the least observed sector of the Southern Ocean. According to the model, the maximum modeled macrozooplankton biomass occurs in the Atlantic and Indian sectors of the Southern Ocean (Figure 3). In the Pacific sector, the model results suggest lower macrozooplankton biomass (Figure 3c). The latitudinal patterns of macrozooplankton biomass distribution are fairly similar between our simulation and MAREDAT. The biomass is relatively constant across latitudes in the Indian sector, increases from south to north in the Atlantic sector, and has a peak around 65°S in the Pacific sector of the Southern Ocean (Figure 3b). The maximum macrozooplankton biomass occurs around the Antarctic Peninsula in MAREDAT and the model reproduces the same order of magnitude. However, the model suggests that the maximum biomass is located in the central Atlantic sector.

Implementing a new zooplankton group reduces the mismatch with the observed chlorophyll and nutrient concentrations. In the CTRL, there is a positive bias (up to 1 mg chl m^{-3}) compared to the satellite chlorophyll concentrations in the coastal areas of the Southern Ocean. In MACROZOO_ALL this positive bias is reduced to 0.3 mg chl m^{-3} (Figure S4 in Supporting Information S1). This is also in agreement with the role of krill grazing on the Southern Ocean ecosystem described by (Smetacek et al., 2004). When CTRL and WOA silicic acid (DSi) concentrations are compared, a negative bias is revealed, especially close to Antarctica. The negative bias is around 12 mmol DSi m^{-3} between 50 and 64°S and 30–100 m depth (Figure S3e in Supporting Information S1). DIN shows positive and negative biases, with a negative DIN bias of up to 8 mmol m^{-3} between 50 and 60°S and 0–150 m depth in the CTRL simulation (Figure S2g in Supporting Information S1). A positive bias for DIN (up to 6 mmol DSi m^{-3}) is present between 60 and 64°S and 100–150 m depth. In MACROZOO_ALL, there is a slight increase in DSi (up to 5 mmol m^{-3}) south of 50°S in the upper 100 m. This spatial pattern shows similarity with the changes in diatom chlorophyll concentrations (Figure S1 in Supporting Information S1), presumably as a result of the decreasing diatom abundance. In MACROZOO_ALL, there is a notable decrease (up to 1 mmol m^{-3}) in nitrate concentration between 60 and 64°S and 100–150 m depth.

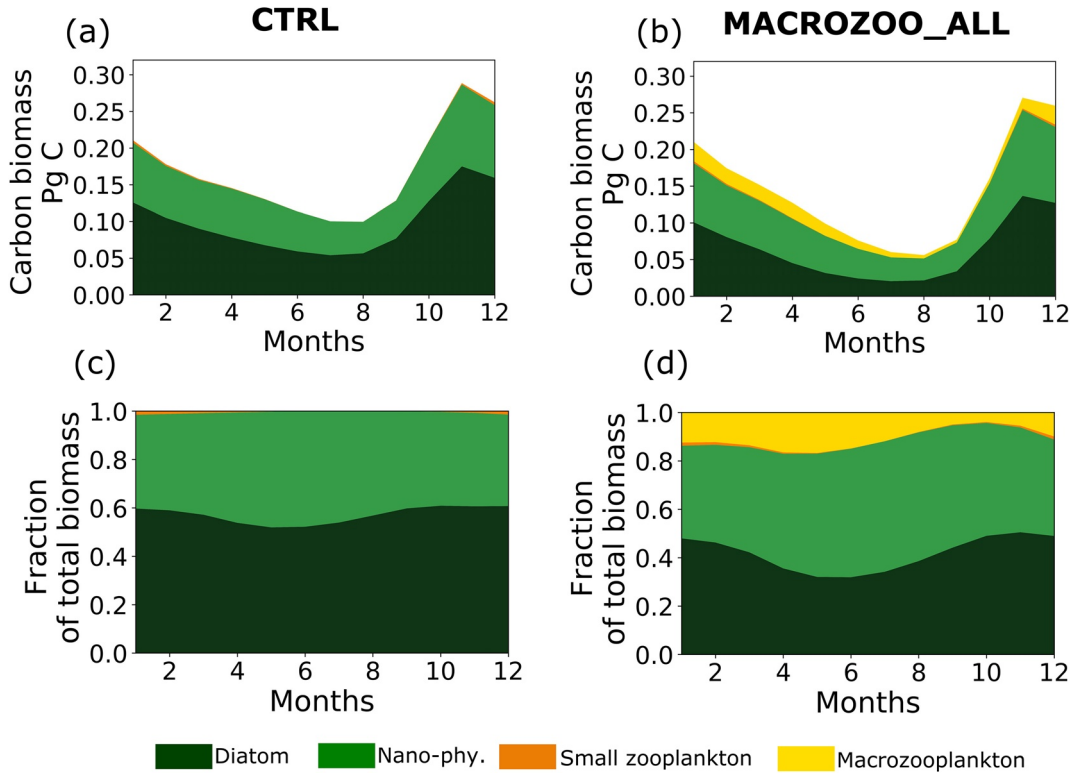

Figure 4. Seasonal cycle of carbon biomass (a and b) and share (c and d) of phytoplankton and zooplankton contribution to the total carbon biomass integrated over the upper 150 m south of 50°S. First column control simulation, second column MACROZOO_ALL.

3.2. Phytoplankton and Zooplankton Community Composition in the Southern Ocean

In the control simulation, the shares of nanophytoplankton, diatoms, and zooplankton of the total carbon biomass amount to 41.6%, 57.8%, and 0.6% of the total carbon biomass south of 50°S, respectively. In MACROZOO_ALL, the fraction of diatoms decreases to 45.9% of total carbon biomass due to increased grazing pressure, while the fraction of nanophytoplankton increases to 44.8%. Small zooplankton remains at 0.6% and macrozooplankton contributes 8.7% to the total carbon biomass. Hence, the total share of grazers increases from 0.6% to 9.3% of the total carbon biomass in the modeled ecosystem.

The total carbon biomass reaches its maximum (0.29 Pg C in CTRL, 0.27 Pg C in MACROZOO_ALL) in November and its minimum between June and August in both simulations. While the grazer biomass reaches its maximum <0.01 Pg C in December in CTRL, the maximum biomass is increased (0.03 Pg C) in MACROZOO_ALL and occurs in December and January (Figures 4a and 4b). Diatoms contribute the largest fraction of the total biomass in both CTRL and MACROZOO_ALL throughout the year. In CTRL, the fractions of diatoms, nanophytoplankton, and the small zooplankton group vary over the year, with values between 52%-61% (diatoms), 38%–48% (nanophytoplankton), and 0.03%–1.4% (zooplankton), respectively. In MACROZOO_ALL, the fraction of diatoms varies at lower levels between 32% and 50%. Nanophytoplankton exhibit a slightly increased variability between 35% and 54%. The new macrozooplankton group contributes between 4% (in October) and 17% (in April-May) to the total biomass (Figures 4c and 4d). While nanophytoplankton prevails between 50°S and 60°S in both simulations, diatoms are the dominant phytoplankton group south of 60°S (Figures 5e and 5f).

While there are some changes in the biomass of phytoplankton groups, as described above, the main characteristics of the seasonal cycle in CTRL, as diagnosed from monthly mean model output, are preserved in the MACROZOO_ALL set-up. In both simulations, the spring peak takes place in November, and the minimum biomass occurs from July to August (Figure 4). The phenology thus follows similar patterns as in the preceding model version with the magnitude of NPP comparable to satellite-derived estimates, and a fast and early

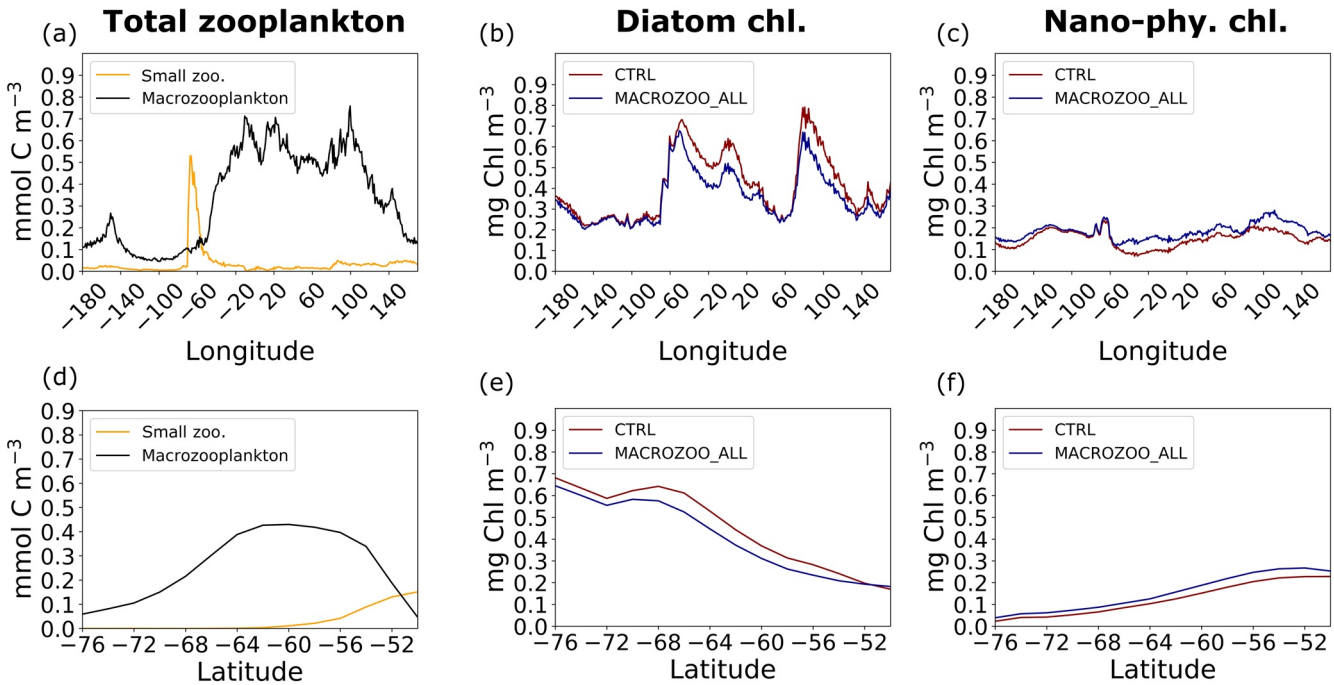

Figure 5. Annual mean surface concentrations of zooplankton biomass and phytoplankton chlorophyll that have then been averaged in the meridional (first row) and zonal (second row) directions. Panels (a) and (d) depict the annual mean zooplankton biomass in MACROZOO_ALL, panels (b) and (e) diatom chlorophyll in control simulation (CTRL) and MACROZOO_ALL, and (c) and (f) nanophytoplankton chlorophyll in CTRL and MACROZOO_ALL.

spring bloom (see analysis in Schourup-Kristensen et al., 2014). One notable difference is a one month shift of spring maximum NPP in the Atlantic, Indian and Pacific sectors and a slightly lower NPP in the Atlantic sector (annual mean is 160 mg C m^{-2} day^{-1} in new simulations) compared to the results in Schourup-Kristensen et al. (2014) that we relate to the parameterization of photodamage used here (Álvarez et al., 2018). A detailed analysis of phytoplankton bloom phenology is beyond the scope of this study and would require higher frequency model output.

Macrozooplankton carbon biomass is higher (0.02–0.025 Pg C) between December and April when sea-ice extent is decreasing (minimum in March 3.1 km^{-2}, Figure S5c in Supporting Information S1). After April, macrozooplankton biomass continues to decrease and reaches minimum values (0.004 Pg C) when the sea-ice extent is reaching maximum (18.6 km^{-2} in September, Figure S5c in Supporting Information S1). In nature, different life stages of macrozooplankton (krill) can use the sea ice as a refuge area or sea-ice algae as a winter food source and increase survival capability (Meyer, 2012). Since we do not represent these mentioned processes, winter macrozooplankton biomass is almost 10 times lower than summer macrozooplankton biomass. The seasonal evolution of macrozooplankton biomass expectedly follows the phytoplankton biomass.

The surface distribution of phytoplankton and zooplankton along longitude and latitude is illustrated in Figure 5. Diatom chlorophyll concentration exhibits a maximum of 0.7 mg chl m^{-3} around 60°W, near the Antarctic Peninsula. It reaches another peak around 100°E (in the Indian sector) and is generally lower in the Pacific sector (0.3–0.4 mg chl m^{-3}, Figure 5b). The surface zooplankton concentrations follow a similar pattern in the east-west direction. The small zooplankton group increases in abundance going northwards (Figure 5d) and peaks around 60°W (0.5 mmol C m^{-3}, Figure 5a). The macrozooplankton carbon concentration reaches a plateau of 0.7 mmol C m^{-3} between 20°W (in the Atlantic sector) and 100°E (in the Indian sector) and it is the dominant grazer group throughout most of the Southern Ocean (Figures 5a and 5d). The new grazing pressure slightly decreases diatom chlorophyll concentration (by <0.1 mg chl m^{-3}) and increases nano-phytoplankton chlorophyll concentration (by <0.1 mg chl m^{-3}) between 60°W and 100°E (Figures 5b–5f).

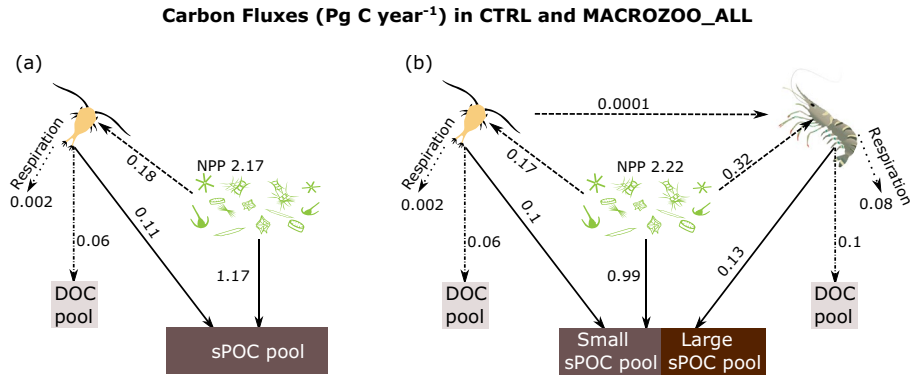

Figure 6. Fluxes between model compartments in (left) CTRL and (right) MACROZOO_ALL: sPOC production via phytoplankton aggregation, mortality, sloppy feeding and fecal pellets of zooplankton groups (solid line), grazing flux to zooplankton (dashed line), DOC production (dashed-dotted line), respiration of zooplanktons (dotted line). DOC: dissolved organic carbon, sPOC: sinking particulate organic carbon, NPP: net primary production.

3.3. Carbon Transfer Pathways in FESOM-REcoM in the Southern Ocean

Carbon fluxes between different ecosystem compartments are presented in Figure 6. Total NPP increased slightly from 2.17 to 2.22 Pg C yr^{-1} in the MACROZOO_ALL simulation compared to CTRL (Figure 6). The grazing flux from primary producers to zooplankton groups is more than doubled with 0.49 Pg C yr^{-1} (22.1% of NPP) in MACROZOO_ALL compared to 0.18 Pg C yr^{-1} (8.3% of total NPP) in CTRL. The contribution of the total zooplankton to total particle formation also doubled from 0.11 Pg C yr^{-1} (8.6% of total particle flux formation) in CTRL to 0.23 Pg C yr^{-1} (18.9%) in MACROZOO_ALL. DOC-excretion by zooplankton increased from 0.06 Pg C yr^{-1} in CTRL to 0.16 Pg C yr^{-1} in MACROZOO_ALL (with 0.10 Pg C yr^{-1} from macrozooplankton). Respiration by both zooplankton groups transfer <0.01 and 0.08 Pg C yr^{-1}, respectively, to the dissolved inorganic carbon pool. In total, macrozooplankton contributes 65% to the total zooplankton grazing flux, 10% to sPOC formation, 63% to DOC production, and 97% to total zooplankton respiration (Figure 6).

The sPOC production by different groups is shown in Figure 7a. In CTRL, the main contribution to sPOC production is from primary producers as a result of aggregation. It is dominated by diatoms (varying from <0.01 in July/August to 0.18 Pg C $month^{-1}$ in November) with a smaller contribution of nanophytoplankton (varying from <0.01 in July to 0.12 Pg C $month^{-1}$ in November). Zooplankton-related sPOC production occurs mostly between November and April and it ranges between 2×10^{-4} to 0.03 Pg C $month^{-1}$ (Figure 7a). In MACROZOO_ALL, phytoplankton aggregation is still the dominant process. In contrast to the control simulation, nanophytoplankton and diatoms now contribute in similar shares to sPOC production via aggregation (diatoms: <0.01 to 0.15 Pg C $month^{-1}$, nanophytoplankton: <0.01 to 0.13 Pg C $month^{-1}$) in MACROZOO_ALL. The sPOC production by the small zooplankton varies between <0.01 and 0.03 Pg C $month^{-1}$ and macrozooplankton sPOC production ranges between <0.01 and 0.02 Pg C $month^{-1}$ (Figure 7b).

Over the course of the year, the fraction of diatom and nanophytoplankton aggregation in sPOC formation pathways peaks in June and July (98.4%) in CTRL. In MACROZOO_ALL, aggregation shows higher contributions in spring/summer with a maximum of 91.6% in November. The contribution of zooplankton (sloppy feeding, mortality, fecal pellets) to sPOC production increases from 1.5%–13.0% in CTRL to 11.8%–39.0% in MACROZOO_ALL. While the zooplankton contribution is lowest (1.5%–5.0%) from May to November in CTRL (Figure 7c), in MACROZOO_ALL it shows a higher contribution throughout the year and has the largest share after the spring/summer phytoplankton bloom (Figure 7d). The relative contribution of macrozooplankton is lowest in November (6%) and highest in April (30%), while the small zooplankton contributes 2%–13% (Figure 7d).

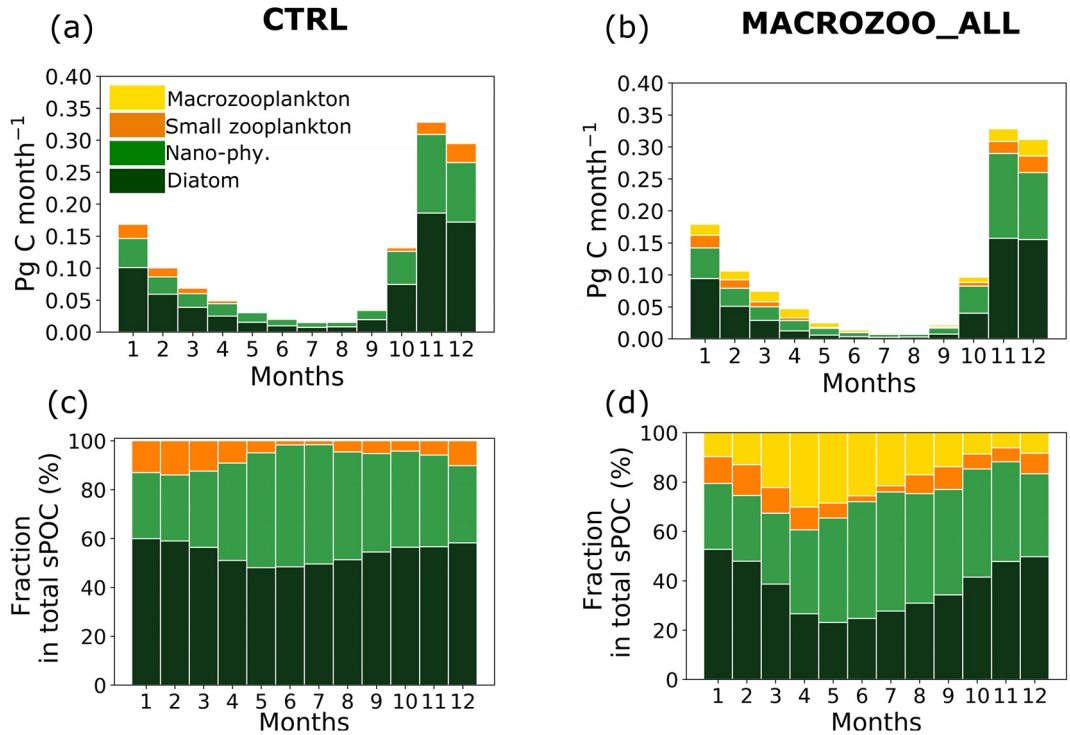

Figure 7. Seasonal cycle of sinking particulate organic carbon (sPOC) production south of 50°S by phyto- and zooplankton groups in absolute and relative terms for both simulations. The sPOC production in CTRL and MACROZOO_ALL (a, b) and fractions of different groups in CTRL and MACROZOO_ALL (c, d). Left column (a, c) shows results in CTRL, and right column (b, d) shows MACROZOO_ALL simulation.

3.4. Particulate Organic Matter Export in the Southern Ocean

Implementation of the macrozooplankton group into the ecosystem model affects the particulate nitrate and carbon export to the deep ocean, and this effect increases with depth (Figure 8). The total amount of exported carbon and nitrogen hardly changes across the 100 m depth level with 0.82 Pg C yr^{-1} and 0.18 Pg N yr^{-1} in CTRL and 0.81 Pg C yr^{-1} and 0.17 Pg N yr^{-1} in MACROZOO_ALL. Depth profiles of exported carbon and nitrogen exhibit similar patterns in both simulations. EP reaches its maximum around 90 m and decreases in deeper layers (Figures 8a and 8b). Carbon export in MACROZOO_ALL increases in almost all depth layers, but especially below 200 m (Figure 8c). This increase reaches 0.05 Pg C yr^{-1} at 1,000 m. In contrast, the exported nitrogen mostly decreases in the upper 200 m and increases by 0.01 PgC yr^{-1} below 200 m in MACROZOO_ALL (Figure 8d).

In addition, we calculated the p-ratio (sPOC production/NPP), s-ratio (EP/sPOC production), and their product e-ratio (EP/NPP) to analyze the export more closely (Laufkötter et al., 2016). The p-ratio describes the efficiency of the particle formation in the ecosystem and the s-ratio is the fraction of particles that escape remineralization at the surface. A higher s-ratio indicates that a larger proportion of formed particles sinks through the 100 m horizon, that is, a smaller amount of particles is remineralized. The s-ratio slightly increases (from 0.67 to 0.70) due to the higher sinking rate of the large detritus class. The p-ratio and e-ratio decrease from 0.58 to 0.55 and 0.39 to 0.38, respectively compared to CTRL. The change of the p-ratio and e-ratio is a result of an increase in NPP in MACROZOO_ALL.

In regions where macrozooplankton is abundant, carbon and nitrogen export across 1,000 m depth almost double in the MACROZOO_ALL simulation (Figures 9a and 9b). While in the CTRL carbon export across 1,000 m mostly varies between 2 and 8 g C m^{-2} yr^{-1}, it can reach values up to 15 g C m^{-2} yr^{-1} in MACROZOO_ALL. Similarly, nitrogen export across 1,000 m reaches peak values of 2.6 g C m^{-2} yr^{-1} in MACROZOO_ALL, 73% higher than the 1.5 g C m^{-2} yr^{-1} in CTRL. These higher values occur in places with high macrozooplankton concentrations at the surface. After implementing macrozooplankton, the exported material becomes richer in terms

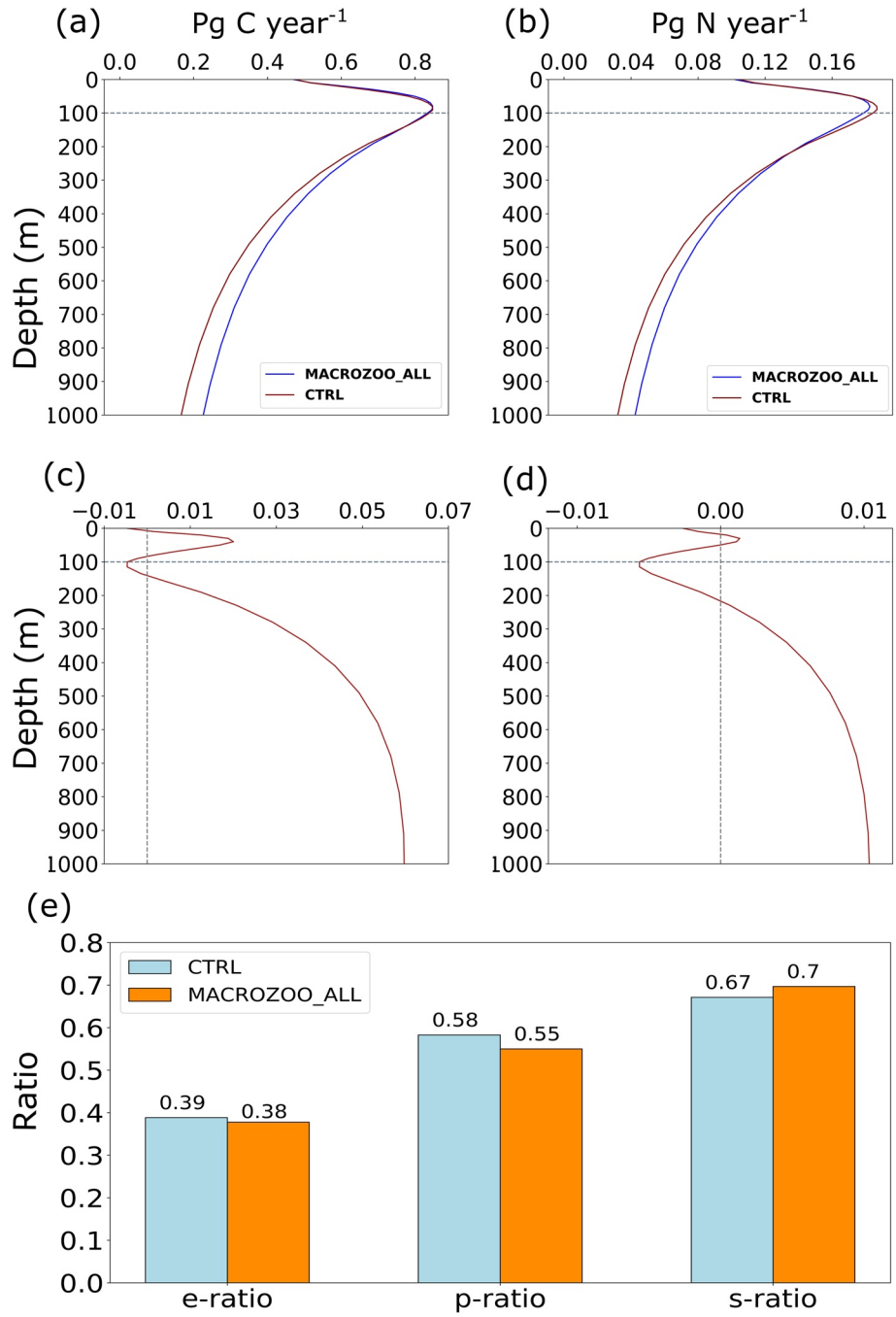

Figure 8. Annual export fluxes of particulate organic carbon (POC) and nitrogen (PON) south of 50°S in CTRL (red) and MACROZOO_ALL (blue) (a, b), difference between MACROZOO_ALL and CTRL POC and PON export fluxes (c, d), and annual mean of e-, p- and s-ratios south of 50°S in both simulations (e).

of carbon, and C:N ratios increase up to 5.5 (Figure 9c). It is directly related to the carbon to nitrogen ratio of the large detritus class which varies between 6.0 (minimum) and 6.7 (maximum) in different depth levels (Figure S3 in Supporting Information S1).In addition, the transfer efficiency (EP_{1000}/EP_{100}) relating the sequestration flux at 1,000 m to the export flux (Passow & Carlson, 2012) is three times higher at places with higher macrozooplankton concentration compared to the CTRL simulation, due to the high sinking rates of particles and the carbon-enrichment of macrozooplankton fecal pellets (Figure 9d).

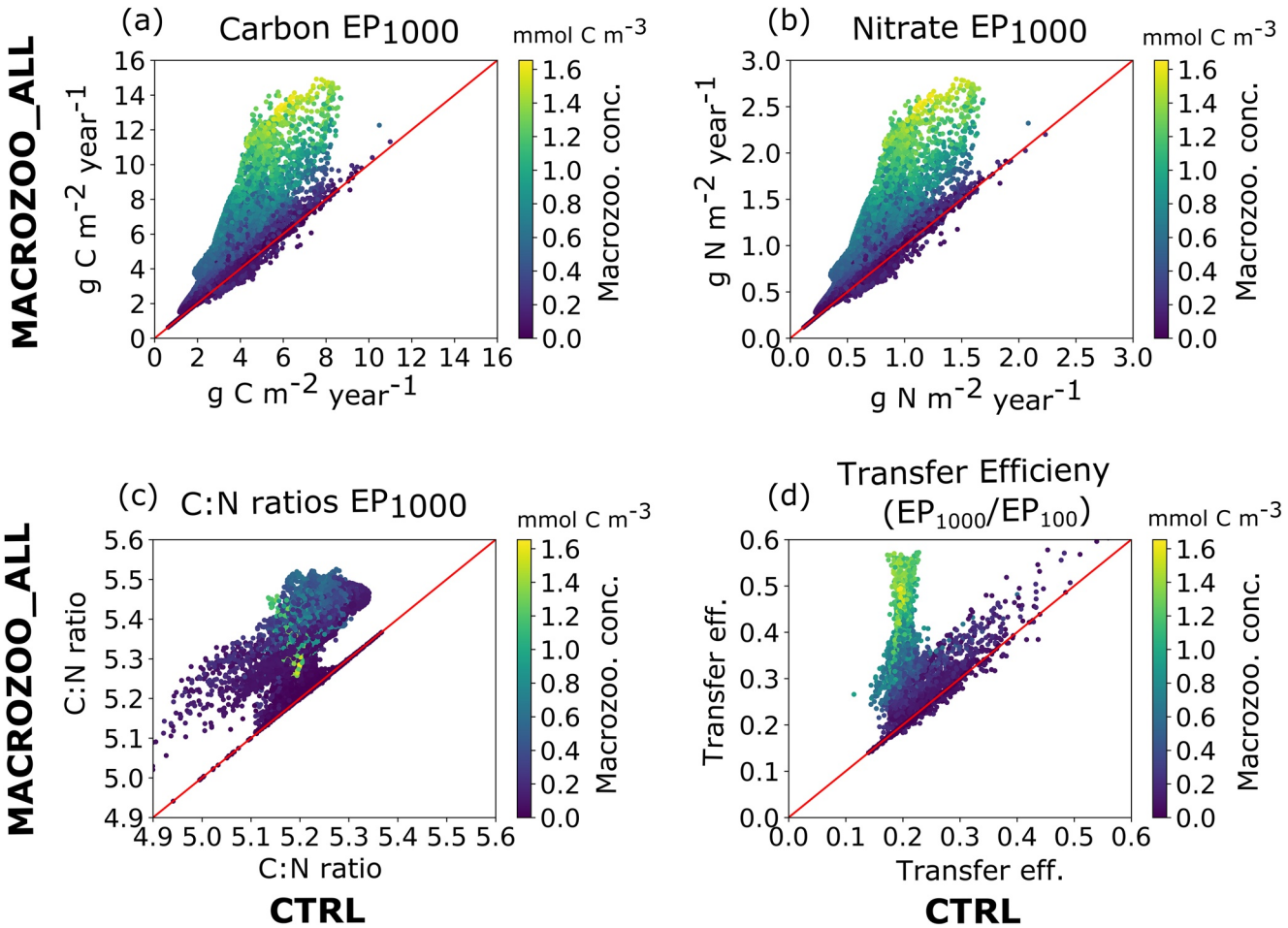

Figure 9. Point-wise comparison of annual mean carbon and nitrogen export at 1,000 m, (c)N ratio of exported material and transfer efficiency between CTRL (*x*-axis) and MACROZOO_ALL (*y*-axis) south of 50°S. Each dot represents one model grid point. Annual export of C and N at 1,000 m (a, b), C:N ratios of exported material (c) and transfer efficiency (EP_{1000}/EP_{100}) (d). The red line represents the one-to-one line in the plots. The color shading indicates the surface macrozooplankton concentration.

Increases in the transfer efficiency show spatial differences. In MACROZOO_ALL, the highest transfer efficiency (more than 50%) is located in the Atlantic and Indian sectors of the Southern Ocean (Figures 10a and 10b) where high macrozooplankton biomass (Figures 3a) occurs. This is due to the macrozooplankton-related larger particle class. Also, the difference between carbon and nitrogen transfer efficiencies (Figure 10f) is higher (up to 0.05) which indicates carbon-enrichment of macrozooplankton fecal pellets. In CTRL, the maximum transfer efficiency is located in the Pacific sector (up to 25%, Figure 10a). Differences between carbon and nitrogen transfer efficiencies are positive, with values up to 0.02 (Figure 10c).

3.5. Disentangling Processes Contributing to Changes in Carbon Pathways

In this section, we analyze the effects of different aspects of the macrozooplankton representation. In Table 3, annual total NPP, EP, and sPOC formation are presented for the various simulations. All simulations with macrozooplankton have in common that there is a 2%–6% increase in total NPP and a 1%–17% decrease in EP at 100 m in comparison to the CTRL simulation (Table 3). Total sinking particle formation decreases by 4.6%–9% in the macrozooplankton simulations, while the contribution of the zooplankton groups to sPOC formation increases from 8.5% (CTRL) to 14%–19% (macrozooplankton simulations, Table 3). In all simulations with the macrozooplankton group, diatom chlorophyll concentrations decrease (Figure 5), and consequently, the contribution of diatoms to sPOC formation decreases from 57% in CTRL to 47% in the simulations with

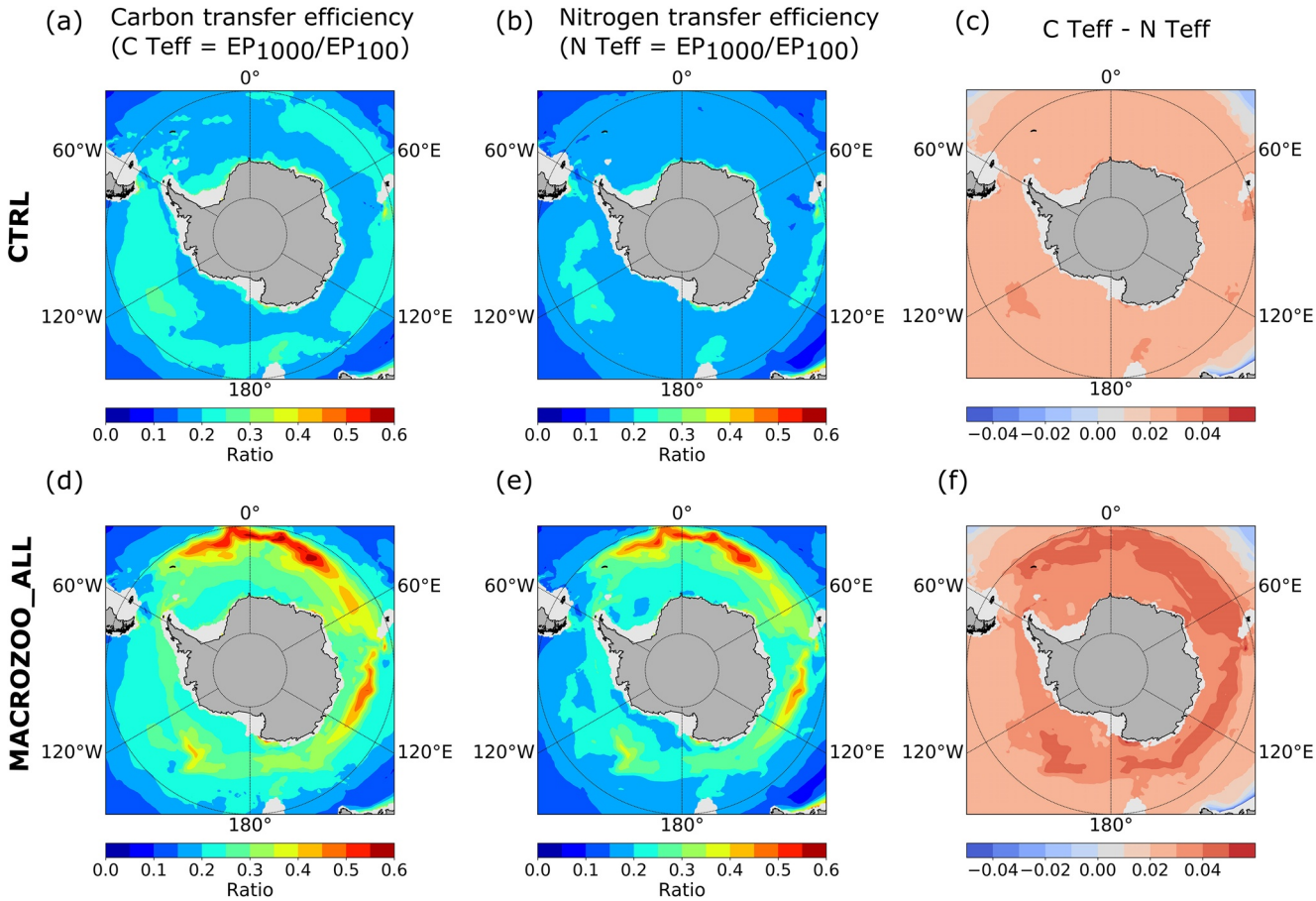

Figure 10. Spatial distributions of (a, d) carbon transfer efficiency (C Teff = EP_{1000}/EP_{100}), (b, e) nitrogen transfer efficiency (N Teff = EP_{1000}/EP_{100}) and (c, f) difference between C Teff and N Teff in CTRL (first row) and MACROZOO_ALL (second row). EP_{1000}: export flux at 1,000 m. EP_{100}: export flux at 100 m.

macrozooplankton. The new macrozooplankton group helps to reduce a probably overly large role of diatom aggregation that was found in the model without macrozooplankton. When we implement only the bare new macrozooplankton group (MACROZOO) to the model, NPP increases by 0.13 Pg C yr^{-1}, as nutrients are kept in the surface layer via excretion by macrozooplankton. The new large detritus class for the macrozooplankton group in the model (MACROZOO_2DET) causes a 35% increase in EP_{1000} compared to MACROZOO. After implementing particle grazing by the zooplankton groups (MACROZOO_DETGRAZ), NPP increases 0.01 Pg C yr^{-1} compared to MACROZOO_2DET. EP_{100} decreases in the simulations in MACROZOO, MACROZOO_2DET, and MACROZOO_DETGRAZ as the grazed biomass also builds up macrozooplankton biomass and

Table 3
Spatially-Integrated Net Primary Production (NPP), Carbon Export Flux at 100 m (EP_{100}) and 1,000 m (EP_{1000}), Total Particle Formation (Total sPOC), Total Phytoplankton Aggregation (Total agg.) and Total Particle Formation by the Zooplankton Groups (sPOC zoo.) South of 50°S in Different Simulations

Simulation	NPP	EP_{100}	EP_{1000}	Total sPOC	Total agg.	sPOC zoo.
CTRL	2.17	0.82	0.16	1.28	1.17	0.11
MACROZOO	2.30	0.77	0.14	1.19	0.99	0.2
MACROZOO_2DET	2.28	0.77	0.19	1.17	0.96	0.21
MACROZOO_DETGRAZ	2.29	0.77	0.19	1.18	0.97	0.21
MACROZOO_ALL	2.22	0.81	0.22	1.22	0.99	0.23

Note. All fluxes are in units Pg C yr^{-1}.

is redistributed via excretion and respiration. When representing fecal pellets with a high C:N ratio explicitly for the macrozooplankton group, macrozooplankton sPOC production and hence export production increase and compensate for the EP decrease due to decreased particle formation. NPP still increases due to the fast recycling of nutrients by the zooplankton group in MACROZOO_ALL, but to a smaller amount than in MACROZOO as part of this effect is compensated by the additional nutrient loss via fecal pellets. The export flux at 1,000 m increases by 0.06 Pg C yr^{-1} when all processes are included (MACROZOO_ALL). This is a pertinent feature in all simulations with the large detritus class (MACROZOO_2DET, MACROZOO_DETGRAZ). The carbon transfer efficiency (EP_{1000}/EP_{100}) south of 50°S increases from 19% (CTRL, MACROZOO) to 25%–27% in the simulations with the large detritus class.

4. Discussion

In this modeling study, we analyze the effect of implementing a macrozooplankton functional type on biogeochemical processes with a focus on the biological carbon pump in the Southern Ocean. Based on our results, annual macrozooplankton sPOC production amounts to more than 10% of total sPOC production in the Southern Ocean (south of 50°S), and carbon transfer efficiency (EP_{1000}/EP_{100}) reaches up to 50% in the areas with high surface macrozooplankton density (Figure 9). Additionally, having macrozooplankton represented in the model enhances the recycling of nutrients in the surface layers, thus increasing NPP.

Our results indicate that macrozooplankton plays an important role in particulate organic carbon production and export efficiency. The seasonal contribution of macrozooplankton to sPOC production (11.8%–39.0%, Figure 7) matches the range observed in field studies (Turner, 2015, highly variable, mostly <40%). In the MACROZOO_ALL simulation, 15.3% of total carbon export at 100 m (0.12 Pg C yr^{-1}, Figure 8) originates from macrozooplankton-related processes in the Southern Ocean. South of 60°S, the modeled total macrozooplankton carbon export is 0.29 Pg C yr^{-1}, which is at the upper end of the reported range from satellite-based estimates (Belcher et al., 2019, 0.09 to 0.29 Pg C yr^{-1}). In the model, macrozooplankton contributes 0.042 Pg C yr^{-1} or 14.3% to the POC flux at 100 m south of 60°S, in agreement with the estimate of 0.039 Pg C yr^{-1} on average, corresponding to 12.5%–43.3% of POC flux by Belcher et al. (2019). REcoM now captures the typical shift from a dominance of phytodetrital aggregates in spring to zooplankton fecal pellets later in the year which was reported for a subantarctic site (Ebersbach & Trull, 2008; Laurenceau-Cornec et al., 2015; Rembauville et al., 2015, Figure 7d).

A pertinent feature of REcoM-2 is its low zooplankton biomass and zooplankton contribution to POC production in the Southern Ocean, in comparison to other biogeochemical models such as BEC and PISCES (Laufkötter et al., 2016). After implementing the macrozooplankton group, the zooplankton share of modeled total biomass increases from 0.6% to 9.3% in the upper 150 m along with the complexity of zooplankton representation (particle grazing, fecal pellet production). This is the first step to a more realistic description of particle formation and destruction processes.

Our estimated macrozooplankton biomass in the upper ocean is in the same range as in the global macrozooplankton dataset MAREDAT. The model simulates maximum macrozooplankton biomass in the Atlantic and Indian sectors of the Southern Ocean and lowers biomass in the Pacific sector, roughly following the chlorophyll distribution (Figure 3). This distribution pattern generally matches observations of Antarctic krill biomass (Atkinson et al., 2004; Siegel, 2016). The modeled biomass maximum occurs in the central Atlantic sector rather than near the Antarctic Peninsula as in MAREDAT, which may be explained by the food availability for the macrozooplankton group in the model. The comparison is hampered by the much higher density of observations near the Antarctic Peninsula. Since we do not include swarm forming and vertical migration behavior of macrozooplankton the model captures the mean biomass by design rather than the patches of very high biomass densities in MAREDAT (Figure 3).

The presence of macrozooplankton affects the biomass of primary producers (Figure 4) and, thus, the chlorophyll concentrations (Figure 5) in the model simulations. There is a modest shift from diatoms to nanophytoplankton, but diatoms remain the dominant phytoplankton PFT. Annual mean diatom chlorophyll at the surface decreases by 10% from 0.40 to 0.36 mg chl m^{-3} and nanophytoplankton chlorophyll increases by 20% from 0.15 to 0.18 mg chl m^{-3}. However, the implementation of macrozooplankton does not lead to a drastic reduction in summer

(November to January) chlorophyll concentrations in the Pacific sector of the Southern Ocean as in Le Quéré et al. (2016). This discrepancy can be explained by differences in the latitudinal macrozooplankton biomass distribution between the two models due to different temperature functions (Le Quéré et al., 2016). The maximum annual mean macrozooplankton biomass at the surface occurs closer to the Antarctic continent (between 54°S and 64°S) in the FESOM-REcoM simulations (Figure 3). Since macrozooplankton is parameterized to mimic the temperature tolerance of Antarctic krill in our study, we do not intend to represent macrozooplankton biomass in the warmer regions. In the simulations with macrozooplankton, the model bias of observational nutrient concentrations (Garcia et al., 2018) was slightly reduced in different depth levels in the Southern Ocean (Figure S2 in Supporting Information S1). One reason for this change is a shift in phytoplankton composition (decrease in diatom and increase in nanophytoplankton biomass). Another reason is the recycling of nitrogen and iron by macrozooplankton via excretion, thus retaining nutrients in the surface layer. As the excretion of iron is modeled via a fixed Fe:N ratio, the magnitude of the nutrient recycling effect and the importance of krill in the iron cycling might be underestimated (Tovar-Sanchez et al., 2007).

Our results highlight the important role of macrozooplankton in the carbon and nutrient cycles of the Southern Ocean. The model further supports that macrozooplankton fecal pellet production is an important component of the export flux of the Antarctic biological carbon pump in the Southern Ocean (Belcher et al., 2019; Cavan et al., 2019). Representations of zooplankton loss terms and their contribution to sinking particles are considerably different in ocean biogeochemical models (Laufkötter et al., 2016). The representation of carbon-rich fecal pellets and fast-sinking large particles in our model are crucial macrozooplankton characteristics that lead to a high transfer efficiency of carbon. In agreement with Passow and Carlson (2012), our model results show that macrozooplankton increase carbon-rich particle sinking across 1,000 m.

This particular and important role of polar macrozooplankton may, however, change in the future. Climate change and fisheries could impact krill abundance negatively (Atkinson et al., 2019; Brooks et al., 2018; Klein et al., 2018). Because of the projected decline of krill, the ratio of phytodetrital aggregates to fecal pellets could increase in the future (Cavan et al., 2019) and the efficient particulate organic carbon transfer via macrozooplankton activity could decrease. This scenario is similar to our control model simulation. In such a case, carbon sequestration flux below 1,000 m could substantially decrease in the future.

Our results also suggest that macrozooplankton stimulates net primary production. This feature is in agreement with the reported role of krill in the Southern Ocean (Coello-Camba et al., 2017; Smetacek, 2008). Krill supports phytoplankton growth by releasing nutrients via excretion, sloppy feeding, and egestion (Lehette et al., 2012). This effect might be even larger when considering varying Fe:N ratios (Tovar-Sanchez et al., 2007). Mass migration of krill swarms could also mix nutrients and stimulate primary production (Cavan et al., 2019), although our model does not include this particular feature (migration). Thus, the reported effect on NPP may be underestimated.

In our model, macrozooplankton is parameterized based on specific characteristics of Antarctic krill. However, salps could replace krill in case of reported and projected declines in krill biomass (Atkinson et al., 2004, 2019; Huang et al., 2011; Pakhomov & Hunt, 2017). One of the main differences between krill and salps is the feeding strategy. While krill prefers filter-feeding on diatoms and smaller zooplankton (Smetacek et al., 2004), salps are non-selective filter-feeders (Henschke et al., 2016). This difference could substantially affect the modeled and real phytoplankton composition in the Southern Ocean and may have a direct impact on the use of macronutrients (Plum et al., 2020). Besides, microphagous feeding of salps might pack nanophytoplankton to larger particles and thus create food items for zooplankton (Iversen et al., 2017). This could have an impact on the spatial distribution of zooplankton in the (modeled) ecosystem.

Furthermore, a shift from krill to salp dominance could impact the POC export fluxes. Since salps can form ”swarms” (due to budding) and produce fast-sinking pellets, they can partially fill the ecological niche of krill (Cavan et al., 2019). However, it remains unresolved whether POC export would increase if salps partially replace krill, or not. Although POC flux is thought to be high during high salp abundance, fragmentation can reduce their sinking speed and contribution to carbon export considerably (Henschke et al., 2016; Iversen et al., 2017). Thus, additional modeling work is needed to resolve the impacts of a potential shift from krill to salps.

Our model takes into account the key characteristics of Antarctic macrozooplankton. While we are confident that the representation of macrozooplankton is solid and captures first-order effects for Southern Ocean biogeochemistry, second-order processes are not taken into account here. For example, a more advanced relationship between the macrozooplankton and sea ice could improve the model results. First, it might improve the seasonal development of macrozooplankton biomass since winter sea ice extent is important for recruitment success and population size (Siegel & Loeb, 1995). Second, implementation of sea-ice algae as an additional food source for the macrozooplankton group (Meyer, 2012; Meyer et al., 2017; Schmidt et al., 2014) could affect the spatial and temporal distribution of macrozooplankton biomass. Also, unrepresented life stages and life-cycle strategies such as molting and resting stages could fundamentally affect nutrient cycles (Everett et al., 2017). In addition, modeling active carbon transport via zooplankton vertical migration is important for carbon export estimates (Archibald et al., 2019). Further steps to represent vertical migration could amplify the role of macrozooplankton in the modeled carbon cycle.

5. Conclusion

In summary, representing macrozooplankton as a plankton functional type and including large rapidly-sinking particles in a biogeochemical model has a strong impact on major carbon pathways in the modeled Southern Ocean. These carbon-rich particles increase carbon transfer to greater depths, especially below the twilight zone. Concurrently, macrozooplankton (krill) play an important role as "gardeners," as the excretion of micro- and macronutrients enhances their recycling in the surface layer. However, the projected decline of macrozooplankton biomass or a shift from a krill- to a salp-dominated ecosystem could weaken the sequestration flux and change the recycling of nutrients. Thus, representing components of the planktonic community and their impacts on carbon cycling is important to improve future projections of carbon cycling.

Data Availability Statement

MAREDAT is available on https://doi.org/10.1594/PANGAEA.777398 and WOA18 products are available on https://www.nodc.noaa.gov/OC5/woa18/woa18data.html. The authors acknowledge open access to the data sets "Global distributions of epipelagic macrozooplankton abundance and biomass—Gridded data product (NetCDF)—Contribution to the MAREDAT World Ocean Atlas of Plankton Functional Types" and World Ocean Atlas 2018 nutrient products. The model results can be downloaded from https://doi.pangaea.de/10.1594/PANGAEA.935006.

Acknowledgments
The authors thank the editor Dr. Nadia Pinardi, reviewer Dr. Mark Hague and one anonymous reviewer for their valuable comments and suggestions. This research was supported under the Initiative and Networking Fund of the Helmholtz Association (Helmholtz Young Investigator Group Marine Carbon and Ecosystem Feedbacks in the Earth System [MarESys], grant number VH-NG-1301). Open access funding enabled and organized by Projekt DEAL.

References

Álvarez, E., Thoms, S., & Völker, C. (2018). Chlorophyll to carbon ratio derived from a global ecosystem model with photodamage. *Global Biogeochemical Cycles*, *32*(5), 799–816. https://doi.org/10.1029/2017gb005850

Anderson, T. R., Hessen, D. O., Mitra, A., Mayor, D. J., & Yool, A. (2013). Sensitivity of secondary production and export flux to choice of trophic transfer formulation in marine ecosystem models. *Journal of Marine Systems*, *125*, 41–53. https://doi.org/10.1016/j.jmarsys.2012.09.008

Archibald, K. M., Siegel, D. A., & Doney, S. C. (2019). Modeling the impact of zooplankton diel vertical migration on the carbon export flux of the biological pump. *Global Biogeochemical Cycles*, *33*(2), 181–199. https://doi.org/10.1029/2018GB005983

Arrigo, K. R., Worthen, D. L., & Robinson, D. H. (2003). A coupled ocean-ecosystem model of the Ross Sea: 2. Iron regulation of phytoplankton taxonomic variability and primary production. *Journal of Geophysical Research*, *108*(C7), 3231. https://doi.org/10.1029/2001JC000856

Arteaga, L., Haëntjens, N., Boss, E., Johnson, K. S., & Sarmiento, J. L. (2018). Assessment of export efficiency equations in the Southern Ocean applied to satellite-based net primary production. *Journal of Geophysical Research: Oceans*, *123*(4), 2945–2964. https://doi.org/10.1002/2018JC013787

Atkinson, A., Hill, S. L., Pakhomov, E. A., Siegel, V., Reiss, C. S., Loeb, V. J., et al. (2019). Krill (*Euphausia superba*) distribution contracts southward during rapid regional warming. *Nature Climate Change*, *9*(2), 142–147. https://doi.org/10.1038/s41558-018-0370-z

Atkinson, A., Meyer, B., Stübing, D., Hagen, W., Schmidt, K., & Bathmann, U. V. (2002). Feeding and energy budgets of Antarctic krill *Euphausia superba* at the onset of winter-II. Juveniles and adults. *Limnology & Oceanography*, *47*(4), 953–966. https://doi.org/10.4319/lo.2002.47.4.0953

Atkinson, A., Schmidt, K., Fielding, S., Kawaguchi, S., & Geissler, P. A. (2012). Variable food absorption by Antarctic krill: Relationships between diet, egestion rate and the composition and sinking rates of their fecal pellets. *Deep-Sea Research Part II Topical Studies in Oceanography*, *59–60*, 147–158. https://doi.org/10.1016/j.dsr2.2011.06.008

Atkinson, A., Shreeve, R. S., Hirst, A. G., Rothery, P., Tarling, G. A., Pond, D. W., et al. (2006). Natural growth rates in Antarctic krill (*Euphausia superba*): II. Predictive models based on food, temperature, body length, sex, and maturity stage. *Limnology & Oceanography*, *51*(2), 973–987. https://doi.org/10.4319/lo.2006.51.2.0973

Atkinson, A., Siegel, V., Pakhomov, E., & Rothery, P. (2004). Long-term decline in krill stock and increase in salps within the Southern Ocean. *Nature*, *432*(7013), 100–103. https://doi.org/10.1038/nature02996

Atkinson, A., Siegel, V., Pakhomov, E. A., Jessopp, M. J., & Loeb, V. (2009). A re-appraisal of the total biomass and annual production of Antarctic krill. *Deep-Sea Research Part I Oceanographic Research Papers*, *56*(5), 727–740. https://doi.org/10.1016/j.dsr.2008.12.007

Aumont, O., Ethé, C., Tagliabue, A., Bopp, L., & Gehlen, M. (2015). PISCES-v2: An ocean biogeochemical model for carbon and ecosystem studies. *Geoscientific Model Development*, *8*(8), 2465–2513. https://doi.org/10.5194/gmd-8-2465-2015

Belcher, A., Henson, S. A., Manno, C., Hill, S. L., Atkinson, A., Thorpe, S. E., et al. (2019). Krill faecal pellets drive hidden pulses of particulate organic carbon in the marginal ice zone. *Nature Communications*, *10*(1), 1–8. https://doi.org/10.1038/s41467-019-08847-1

Belcher, A., Tarling, G. A., Manno, C., Atkinson, A., Ward, P., Skaret, G., et al. (2017). The potential role of Antarctic krill faecal pellets in efficient carbon export at the marginal ice zone of the South Orkney Islands in spring. *Polar Biology*, *40*(10), 2001–2013. https://doi.org/10.1007/s00300-017-2118-z

Boyd, P. W., Claustre, H., Levy, M., Siegel, D. A., & Weber, T. (2019). Multi-faceted particle pumps drive carbon sequestration in the ocean. *Nature*, *568*(7752), 327–335. https://doi.org/10.1038/s41586-019-1098-2

Brooks, C. M., Ainley, D. G., Abrams, P. A., Dayton, P. K., Hofman, R. J., Jacquet, J., & Siniff, D. B. (2018). Watch over Antarctic waters. *Nature*, *558*(7709), 177–180. https://doi.org/10.1038/d41586-018-05372-x

Butzin, M., & Pörtner, H. O. (2016). Thermal growth potential of Atlantic cod by the end of the 21st century. *Global Change Biology*, *22*(12), 4162–4168. https://doi.org/10.1111/gcb.13375

Cavan, E. L., Belcher, A., Atkinson, A., Hill, S. L., Kawaguchi, S., McCormack, S., et al. (2019). The importance of Antarctic krill in biogeochemical cycles. *Nature Communications*, *10*(1), 1–13. https://doi.org/10.1038/s41467-019-12668-7

Clarke, A., Quetin, L. B., & Ross, R. M. (1988). Laboratory and field estimates of the rate of faecal pellet production by Antarctic krill, *Euphausia superba*. *Marine Biology*, *98*(4), 557–563. https://doi.org/10.1007/BF00391547

Coello-Camba, A., Llabrés, M., Duarte, C. M., & Agustí, S. (2017). Zooplankton excretion metabolites stimulate Southern Ocean phytoplankton growth. *Polar Biology*, *40*(10), 2035–2045. https://doi.org/10.1007/s00300-017-2123-2

Comiso, J. C., & Nishio, F. (2008). Trends in the sea ice cover using enhanced and compatible AMSR-E, SSM/I, and SMMR data. *Journal of Geophysical Research*, *113*(C2). Retrieved from https://agupubs.onlinelibrary.wiley.com/doi/abs/10.1029/2007JC004257

Dagg, M. J., Urban-Rich, J., & Peterson, J. O. (2003). The potential contribution of fecal pellets from large copepods to the flux of biogenic silica and particulate organic carbon in the Antarctic Polar Front region near 170°W. *Deep-Sea Research Part II Topical Studies in Oceanography*, *50*(3–4), 675–691. https://doi.org/10.1016/S0967-0645(02)00590-8

Downes, S., Farneti, R., Uotila, P., Griffies, S. M., Marsland, S. J., Bailey, D., et al. (2015). An assessment of Southern Ocean water masses and sea ice during 1988–2007 in a suite of interannual CORE-II simulations. *Ocean Modelling*, *94*, 67–94. https://doi.org/10.1016/j.ocemod.2015.07.022

Downes, S., Spence, P., & Hogg, A. (2018). Understanding variability of the Southern Ocean overturning circulation in CORE-II models. *Ocean Modelling*, *123*, 98–109. https://doi.org/10.1016/j.ocemod.2018.01.005

Ebersbach, F., & Trull, T. W. (2008). Sinking particle properties from polyacrylamide gels during the KErguelen Ocean and Plateau compared Study (KEOPS): Zooplankton control of carbon export in an area of persistent natural iron inputs in the Southern Ocean. *Limnology & Oceanography*, *53*(1), 212–224. https://doi.org/10.4319/lo.2008.53.1.0212

Everett, J. D., Baird, M. E., Buchanan, P., Bulman, C., Davies, C., Downie, R., et al. (2017). Modeling what we sample and sampling what we model: Challenges for zooplankton model assessment. *Frontiers in Marine Science*, *4*, 77. Retrieved from https://www.frontiersin.org/article/10.3389/fmars.2017.00077

Fach, B. A., Hofmann, E. E., & Murphy, E. J. (2002). Modeling studies of antarctic krill *Euphausia superba* survival during transport across the Scotia Sea. *Marine Ecology Progress Series*, *231*, 187–203. https://doi.org/10.3354/meps231187

Farneti, R., Downes, S. M., Griffies, S. M., Marsland, S. J., Behrens, E., Bentsen, M., et al. (2015). An assessment of Antarctic Circumpolar Current and Southern Ocean meridional overturning circulation during 1958–2007 in a suite of interannual CORE-II simulations. *Ocean Modelling*, *93*, 84–120. https://doi.org/10.1016/j.ocemod.2015.07.009

Fasham, M. J., Ducklow, H. W., & McKelvie, S. M. (1990). A nitrogen-based model of plankton dynamics in the oceanic mixed layer. *Journal of Marine Research*, *48*(3), 591–639. https://doi.org/10.1357/002224090784984678

Frölicher, T. L., Rodgers, K., Stock, C. A., & Cheung, W. W. (2016). Sources of uncertainties in 21st century projections of potential ocean ecosystem stressors. *Global Biogeochemical Cycles*, *30*, 22–1243. https://doi.org/10.1002/2015GB005338

Garcia, H., Locarnini, R., Boyer, T. P., Antonov, J. I., Baranova, O. K., Zweng, M. M., et al. (2013). World Ocean Atlas 2013 volume 4: Nutrients (phosphate, nitrate, silicate). *NOAA Atlas NESDIS*, *76*, 396.

Garcia, H., Weathers, K., Paver, C., Smolyar, I., Boyer, T., Locarnini, R., et al. (2018). World Ocean Atlas 2018. Volume 4: Dissolved inorganic nutrients (phosphate, nitrate and nitrate+nitrite, silicate). *NOAA Atlas NESDIS*, *84*, 35.

Griffies, S. M., Biastoch, A., Böning, C., Bryan, F., Danabasoglu, G., Chassignet, E. P., et al. (2009). Coordinated ocean-ice reference experiments (cores). *Ocean Modelling*, *26*(1), 1–46. https://doi.org/10.1016/j.ocemod.2008.08.007

Griffies, S. M., Yin, J., Durack, P. J., Goddard, P., Bates, S. C., Behrens, E., et al. (2014). An assessment of global and regional sea level for years 1993–2007 in a suite of interannual CORE-II simulations. *Ocean Modelling*, *78*, 35–89. https://doi.org/10.1016/j.ocemod.2014.03.004

Halfter, S., Cavan, E. L., Swadling, K. M., Eriksen, R. S., & Boyd, P. W. (2020). The role of zooplankton in establishing carbon export regimes in the Southern Ocean—A comparison of two representative case studies in the subantarctic region. *Frontiers in Marine Science*, *7*, 1–8. https://doi.org/10.3389/fmars.2020.567917

Hauck, J., Völker, C., Wang, T., Hoppema, M., Losch, M., & Wolf-Gladrow, D. A. (2013). Seasonally different carbon flux changes in the Southern Ocean in response to the southern annular mode. *Global Biogeochemical Cycles*, *27*(4), 1236–1245. https://doi.org/10.1002/2013GB004600

Henschke, N., Everett, J. D., Richardson, A. J., & Suthers, I. M. (2016). Rethinking the role of salps in the ocean. *Trends in Ecology & Evolution*, *31*(9), 720–733. https://doi.org/10.1016/j.tree.2016.06.007

Hense, I., Timmermann, R., Beckmann, A., & Bathmann, U. V. (2003). Regional ecosystem dynamics in the ACC: Simulations with a three-dimensional ocean-plankton model. *Journal of Marine Systems*, *42*(1–2), 31–51. https://doi.org/10.1016/S0924-7963(03)00063-0

Henson, S. A., Sanders, R., & Madsen, E. (2012). Global patterns in efficiency of particulate organic carbon export and transfer to the deep ocean. *Global Biogeochemical Cycles*, *26*(1), 1. https://doi.org/10.1029/2011GB004099

Hofmann, E. E., & Lascara, C. M. (2000). Modeling the growth dynamics of Antarctic krill *Euphausia superba*. *Marine Ecology Progress Series*, *194*, 219–231. https://doi.org/10.3354/meps194219

Honjo, S. (2004). Particle export and the biological pump in the Southern Ocean. *Antarctic Science*, *16*(4), 501–516. https://doi.org/10.1017/S0954102004002287

Huang, T., Sun, L., Stark, J., Wang, Y., Cheng, Z., Yang, Q., & Sun, S. (2011). Relative changes in krill abundance inferred from antarctic fur seal. *PLoS One*, *6*(11), 11–14. https://doi.org/10.1371/journal.pone.0027331

Iversen, M. H., Pakhomov, E. A., Hunt, B. P., van der Jagt, H., Wolf-Gladrow, D., & Klaas, C. (2017). Sinkers or floaters? Contribution from salp pellets to the export flux during a large bloom event in the Southern Ocean. *Deep-Sea Research Part II Topical Studies in Oceanography*, *138*, 116–125. https://doi.org/10.1016/j.dsr2.2016.12.004

Klein, E. S., Hill, S. L., Hinke, J. T., Phillips, T., & Watters, G. M. (2018). Impacts of rising sea temperature on krill increase risks for predators in the Scotia Sea. *PLoS One*, *13*(1), 1–21. https://doi.org/10.1371/journal.pone.0191011

Kobayashi, S., Ota, Y., Harada, Y., Ebita, A., Moriya, M., Onoda, H., et al. (2015). The JRA-55 reanalysis: General specifications and basic characteristics. *Journal of the Meteorological Society of Japan*, *93*(1), 5–48. https://doi.org/10.2151/jmsj.2015-001

Kurtz, N. T., & Markus, T. (2012). Satellite observations of Antarctic sea ice thickness and volume. *Journal of Geophysical Research*, *117*(C8). https://doi.org/10.1029/2012jc008141

Lancelot, C., Hannon, E., Becquevort, S., Veth, C., & De Baar, H. J. (2000). Modeling phytoplankton blooms and carbon export production in the Southern Ocean: Dominant controls by light and iron in the Atlantic sector in Austral spring 1992. *Deep-Sea Research Part I Oceanographic Research Papers*, *47*(9), 1621–1662. https://doi.org/10.1016/S0967-0637(00)00005-4

Laufkötter, C., Vogt, M., Gruber, N., Aumont, O., Bopp, L., Doney, S. C., et al. (2016). Projected decreases in future marine export production: The role of the carbon flux through the upper ocean ecosystem. *Biogeosciences*, *13*(13), 4023–4047. https://doi.org/10.5194/bg-13-4023-2016

Laurenceau-Cornec, E. C., Trull, T. W., Davies, D. M., Bray, S. G., Doran, J., Planchon, F., et al. (2015). The relative importance of phytoplankton aggregates and zooplankton fecal pellets to carbon export: Insights from free-drifting sediment trap deployments in naturally iron-fertilised waters near the Kerguelen Plateau. *Biogeosciences*, *12*(4), 1007–1027. https://doi.org/10.5194/bg-12-1007-2015

Lauvset, S. K., Key, R. M., Olsen, A., Van Heuven, S., Velo, A., Lin, X., et al. (2016). A new global interior ocean mapped climatology: The 1° 11° GLODAP version 2. *Earth System Science Data*, *8*(2), 325–340. https://doi.org/10.5194/essd-8-325-2016

Lehette, P., Tovar-Sánchez, A., Duarte, C. M., & Hernández-León, S. (2012). Krill excretion and its effect on primary production. *Marine Ecology Progress Series*, *459*, 29–38. https://doi.org/10.3354/meps09746

Le Quéré, C., Buitenhuis, E. T., Moriarty, R., Alvain, S., Aumont, O., Bopp, L., et al. (2016). Role of zooplankton dynamics for Southern Ocean phytoplankton biomass and global biogeochemical cycles. *Biogeosciences*, *13*(14), 4111–4133. https://doi.org/10.5194/bg-13-4111-2016

Maiti, K., Charette, M. A., Buesseler, K. O., & Kahru, M. (2013). An inverse relationship between production and export efficiency in the Southern Ocean. *Geophysical Research Letters*, *40*(8), 1557–1561. https://doi.org/10.1002/grl.50219

Meyer, B. (2012). The overwintering of Antarctic krill, *Euphausia superba*, from an ecophysiological perspective. *Polar Biology*, *35*(1), 15–37. https://doi.org/10.1007/s00300-011-1120-0

Meyer, B., Freier, U., Grimm, V., Groeneveld, J., Hunt, B. P., Kerwath, S., et al. (2017). The winter pack-ice zone provides a sheltered but food-poor habitat for larval Antarctic krill. *Nature Ecology and Evolution*, *1*(12), 1853–1861. https://doi.org/10.1038/s41559-017-0368-3

Meyer, B., Fuentes, V., Guerra, C., Schmidt, K., Atkinson, A., Spahic, S., et al. (2009). Physiology, growth, and development of larval krill *Euphausia superba* in autumn and winter in the Lazarev Sea, Antarctica. *Limnology & Oceanography*, *54*(5), 1595–1614. https://doi.org/10.4319/lo.2009.54.5.1595

Moriarty, R., Buitenhuis, E. T., Le Quéré, C., & Gosselin, M.-P. (2013). Distribution of known macrozooplankton abundance and biomass in the global ocean. *Earth System Science Data*, *5*(2), 241–257. https://doi.org/10.5194/essd-5-241-2013

Nicol, S., Constable, A. J., & Pauly, T. (2000). Estimates of circumpolar abundance of Antarctic krill based on recent acoustic density measurements. *CCAMLR Science*, *7*, 87–99.

Pakhomov, E. A., & Hunt, B. P. (2017). Trans-Atlantic variability in ecology of the pelagic tunicate *Salpa thompsoni* near the Antarctic Polar. *Front. Deep-Sea Research Part II: Topical Studies in Oceanography*, *138*(March), 126–140. https://doi.org/10.1016/j.dsr2.2017.03.001

Passow, U., & Carlson, C. (2012). The biological pump in a high CO_2 world. *Marine Ecology Progress Series*, *470*(2), 249–271. https://doi.org/10.3354/meps09985

Plum, C., Hillebrand, H., & Moorthi, S. (2020). Krill vs salps: Dominance shift from krill to salps is associated with higher dissolved N:P ratios. *Scientific Reports*, *10*(1), 5911. https://doi.org/10.1038/s41598-020-62829-8

Rembauville, M., Blain, S., Armand, L., Quéguiner, B., & Salter, I. (2015). Export fluxes in a naturally iron-fertilized area of the Southern Ocean—Part 2: Importance of diatom resting spores and faecal pellets for export. *Biogeosciences*, *12*(11), 3171–3195. https://doi.org/10.5194/bg-12-3171-2015

Schlitzer, R. (2002). Carbon export fluxes in the Southern Ocean: Results from inverse modeling and comparison with satellite-based estimates. *Deep-Sea Research Part II Topical Studies in Oceanography*, *49*(9–10), 1623–1644. https://doi.org/10.1016/S0967-0645(02)00004-8

Schmidt, K., Atkinson, A., Pond, D. W., & Irel, L. C. (2014). Feeding and overwintering of Antarctic krill across its major habitats: The role of sea ice cover, water depth, and phytoplankton abundance. *Limnology & Oceanography*, *59*(1), 17–36. https://doi.org/10.4319/lo.2014.59.1.0017

Schourup-Kristensen, V., Sidorenko, D., Wolf-Gladrow, D. A., & Völker, C. (2014). A skill assessment of the biogeochemical model REcoM2 coupled to the Finite Element Sea Ice–Ocean Model (FESOM 1.3). *Geoscientific Model Development*, *7*(6), 2769–2802. https://doi.org/10.5194/gmd-7-2769-2014

Séférian, R., Berthet, S., Yool, A., Palmiéri, J., Bopp, L., Tagliabue, A., et al. (2020). Tracking Improvement in Simulated Marine Biogeochemistry Between CMIP5 and CMIP6. *Current Climate Change Reports*, *6*(3), 95–119. https://doi.org/10.1007/s40641-020-00160-0

Sidorenko, D., Wang, Q., Danilov, S., & Schröter, J. (2011). FESOM under coordinated ocean-ice reference experiment forcing. *Ocean Dynamics*, *61*(7), 881–890. https://doi.org/10.1007/s10236-011-0406-7

Siegel, V., Kawaguchi, S., Ward, P., Litvinov, F., Sushin, V., Loeb, V., & Watkins, J. (2004). Krill demography and large-scale distribution in the southwest Atlantic during January/February 2000. Deep-Sea Research Part II. *Topical Studies in Oceanography*, *51*(12–13 SPEC.ISS), 1253–1273. https://doi.org/10.1016/s0967-0645(04)00078-5

Siegel, V., & Loeb, V. (1995). Recruitment of Antarctic krill *Euphausia superba* and possible causes for its variability. *Marine Ecology Progress Series*, *123*(1–3), 45–56. https://doi.org/10.3354/meps123045

Siegel, V., & Watkins, J. L. (2016). Distribution, Biomass and Demography of Antarctic Krill *Euphausia superba*. In V. Siegel (Ed.). *Biology and ecology of the Antarctic krill*. Springer. https://doi.org/10.1007/978-3-319-29279-3

Smetacek, V. (2008). Are declining Antarctic krill stocks a result of global warming or of the decimation of whales? In *Impacts of global warming on polar ecosystems* (pp. 45–83). Fundacion BBVA. Retrieved from https://www.fbbva.es/wp-content/uploads/2017/05/dat/02SMETACEK-SEPARATA.pdf

Smetacek, V., Assmy, P., & Henjes, J. (2004). The role of grazing in structuring Southern Ocean pelagic ecosystems and biogeochemical cycles. *Antarctic Science*, *16*(4), 541–558. https://doi.org/10.1017/S0954102004002317

Steinberg, D. K., & Landry, M. R. (2017). Zooplankton and the ocean carbon cycle. *Annual Review of Marine Science*, *9*(1), 413–444. https://doi.org/10.1146/annurev-marine-010814-015924

Stock, C. A., Dunne, J. P., Fan, S., Ginoux, P., John, J., Krasting, J. P., et al. (2020). Ocean biogeochemistry in GFDL's Earth System Model 4.1 and its response to increasing atmospheric CO_2. *Journal of Advances in Modeling Earth Systems*, *12*(10). https://doi.org/10.1029/2019MS002043

Stock, C. A., Dunne, J. P., & John, J. G. (2014). Global-scale carbon and energy flows through the marine planktonic food web: An analysis with a coupled physical–biological model. *Progress in Oceanography*, *120*, 1–28. https://doi.org/10.1016/j.pocean.2013.07.001

Teschke, M., Kawaguchi, S., & Meyer, B. (2007). Simulated light regimes affect feeding and metabolism of Antarctic krill, *Euphausia superba*. *Limnology & Oceanography*, *52*(3), 1046–1054. Retrieved from https://aslopubs.onlinelibrary.wiley.com/doi/abs/10.4319/lo.2007.52.3.1046

Tovar-Sanchez, A., Duarte, C. M., Hernández-León, S., & Sañudo-Wilhelmy, S. A. (2007). Krill as a central node for iron cycling in the Southern Ocean. *Geophysical Research Letters*, *34*(11), 1–4. https://doi.org/10.1029/2006GL029096

Turner, J. T. (2002). Zooplankton fecal pellets, marine snow and sinking phytoplankton blooms. *Aquatic Microbial Ecology*, *27*, 57–102. https://doi.org/10.3354/Ame027057

Turner, J. T. (2015). Zooplankton fecal pellets, marine snow, phytodetritus and the ocean's biological pump. *Progress in Oceanography*, *130*, 205–248. https://doi.org/10.1016/j.pocean.2014.08.005

Volk, T., & Hoffert, M. I. (1985). Ocean carbon pumps: Analysis of relative strengths and efficiencies in ocean-driven atmospheric CO_2 changes. In *The carbon cycle and atmospheric CO_2: Natural variations Archean to present* (pp. 99–110). American Geophysical Union (AGU). https://doi.org/10.1029/GM032p0099

Waite, A. M., Thompson, P. A., & Harrison, P. J. (1992). Does energy control the sinking rates of marine diatoms? *Limnology & Oceanography*, *37*(3), 468–477. https://doi.org/10.4319/lo.1992.37.3.0468

Wang, Q., Danilov, S., Sidorenko, D., Timmermann, R., Wekerle, C., Wang, X., et al. (2014). The finite element sea ice-ocean model (FESOM) v.1.4: Formulation of an ocean general circulation model. *Geoscientific Model Development*, *7*(2), 663–693. https://doi.org/10.5194/gmd-7-663-2014